AFRL-RY-WP-TR-2008-1239

WELL CONDITIONED FORMULATIONS FOR OPEN SURFACE SCATTERING

John J. Ottusch and John L. Visher

HRL Laboratories, LLC

AUGUST 2008
Final Report

Approved for public release; distribution unlimited.

See additional restrictions described on inside pages

STINFO COPY

AIR FORCE RESEARCH LABORATORY
SENSORS DIRECTORATE
WRIGHT-PATTERSON AIR FORCE BASE, OH 45433-7320
AIR FORCE MATERIEL COMMAND
UNITED STATES AIR FORCE

NOTICE AND SIGNATURE PAGE

Using Government drawings, specifications, or other data included in this document for any purpose other than Government procurement does not in any way obligate the U.S. Government. The fact that the Government formulated or supplied the drawings, specifications, or other data does not license the holder or any other person or corporation; or convey any rights or permission to manufacture, use, or sell any patented invention that may relate to them.

This report was cleared for public release by the USAF 88th Air Base Wing (88 ABW) Public Affairs Office (PAO) and is available to the general public, including foreign nationals. Copies may be obtained from the Defense Technical Information Center (DTIC) (http://www.dtic.mil).

AFRL-RY-WP-TR-2008-1239 HAS BEEN REVIEWED AND IS APPROVED FOR PUBLICATION IN ACCORDANCE WITH ASSIGNED DISTRIBUTION STATEMENT.

*//Signature//	//Signature//
MICHAEL S. GILBERT, Project Manager Signature Technology Branch Sensors Division Sensors Directorate	THOMAS C. HOLCOMBE, Chief Signature Technology Branch Sensor s Division Sensors Directorate

This report is published in the interest of scientific and technical information exchange, and its publication does not constitute the Government's approval or disapproval of its ideas or findings.

*Disseminated copies will show "//Signature//" stamped or typed above the signature blocks.

REPORT DOCUMENTATION PAGE

Form Approved
OMB No. 0704-0188

1. REPORT DATE *(DD-MM-YY)*	2. REPORT TYPE	3. DATES COVERED *(From - To)*
August 2008	Final	30 May 2007 – 31 July 2008

4. TITLE AND SUBTITLE
WELL CONDITIONED FORMULATIONS FOR OPEN SURFACE SCATTERING

5a. CONTRACT NUMBER
FA8650-07-C-7720

5b. GRANT NUMBER

5c. PROGRAM ELEMENT NUMBER
62702E

6. AUTHOR(S)
John J. Ottusch and John L. Visher

5d. PROJECT NUMBER
ARPS

5e. TASK NUMBER
NS

5f. WORK UNIT NUMBER
ARPSNS00

7. PERFORMING ORGANIZATION NAME(S) AND ADDRESS(ES)
HRL Laboratories, LLC
3011 Malibu Canyon Road
Malibu, CA 90265

8. PERFORMING ORGANIZATION REPORT NUMBER
6138

9. SPONSORING/MONITORING AGENCY NAME(S) AND ADDRESS(ES)

Air Force Research Laboratory
Sensors Directorate
Wright-Patterson Air Force Base, OH 45433-7320
Air Force Materiel Command
United States Air Force

Defense Advanced Research Projects Agency (DARPA)
Defense Sciences Office
3701 North Fairfax Drive
Arlington, VA 22203-1714

10. SPONSORING/MONITORING AGENCY ACRONYM(S)
AFRL/RYS

11. SPONSORING/MONITORING AGENCY REPORT NUMBER(S)
AFRL-RY-WP-TR-2008-1239

12. DISTRIBUTION/AVAILABILITY STATEMENT
Approved for public release; distribution unlimited.

13. SUPPLEMENTARY NOTES
 This work was funded in whole or in part by Department of the Air Force Contract FA8650-07-C-7720. The U.S. Government has for itself and others acting on its behalf a paid-up, nonexclusive, irrevocable worldwide license to use, modify, reproduce, release, perform, display, or disclose the work by or on behalf of the U. S. Government.

PAO Case Number: 88 ABW 08-1216; Clearance Date: 20 Nov 2008. The paper contains color.

14. ABSTRACT

The electric field integral equation (EFIE) is a first-kind integral equation formulation that is used to solve a wide variety of electromagnetic scattering problems in the frequency domain. It is the only integral equation that can be applied to both open and closed targets. It is also a poorly conditioned integral equation, which means that solving it using iterative solution methods is generally impractical because the iteration count is uncontrollable and can be very large. This reduces the effectiveness of fast iterative solver methods for solving open surface problems.

This report describes an analytical preconditioner method for the EFIE on open surface PEC targets that converts the EFIE to a well conditioned, second-kind integral equation. We present theory and the results from a numerical implementation. We also discuss a 2d extension of the Poincare-Bertrand identity could be used to develop an explicitly second-kind integral equation for open surface scattering problems.

15. SUBJECT TERMS
electric field integral equation, EFIE, open surface scattering, analytical preconditioner, analytical regularization

16. SECURITY CLASSIFICATION OF:			17. LIMITATION OF ABSTRACT:	18. NUMBER OF PAGES	19a. NAME OF RESPONSIBLE PERSON (Monitor)
a. REPORT	b. ABSTRACT	c. THIS PAGE			Michael S. Gilbert
Unclassified	Unclassified	Unclassified	SAR	64	19b. TELEPHONE NUMBER *(Include Area Code)* (937) 255-9220

Standard Form 298 (Rev. 8-98)
Prescribed by ANSI Std. Z39-18

Contents

List of Figures

List of Tables

1 Executive Summary

Practical scattering problems frequently involve thin metal objects with open edges that can be modeled as perfectly conducting open surface targets. Examples include airborne vehicles with thin fins, horn antennas, and high frequency circuits comprising thin strips of metallization on multi-layer substrates. The standard integral equation formulations for obtaining frequency domain solutions to such open surface scattering problems often lead to linear systems of equations that are impractical to solve numerically – the linear system is either too large to solve in a reasonable amount of time by direct inversion or too ill conditioned to solve by iterative means.

The most commonly used integral equation for solving open surface scattering problems is the electric field integral equation (EFIE). It is the only integral equation that can be applied to both open and closed targets. The only practical way to solve large scattering problems is using iterative solvers in conjunction with operator decomposition methods such as the fast multipole method (FMM). Unfortunately, the EFIE is horribly ill conditioned so the iteration count is uncontrollable and can be very large, thus negating any advantage that may accrue from use of a fast method.

The objective of this program was to produce a new integral equation that is inherently well conditioned and suitable for solving open surface scattering problems. We achieved this goal by developing and implementing an analytic preconditioner for the EFIE. We tested the efficacy of the new formulation on simple test problems, finding that it stabilized and dramatically improved iterative solver performance as compared to conventional numerical preconditioning methods. For example, on the EletroMagnetic Code Consortium (EMCC) triangle-circle target the analytically preconditioned EFIE only required $\sim$30 iterations to achieve convergence as compared to $\sim$50000 for the standard EFIE with a conventional block diagonal preconditioner. In stark contrast to the EFIE, the eigenvalue spectrum of the new formulation has a distinctly second kind character. Consequently, the computed source distribution (i.e., equivalent surface current) is also noticeably smoother.

Our original plan for realizing a numerical implementation of the analytically preconditioned EFIE involved using a $2d$ extension to the $1d$ Poincaré-Bertrand identity (PBI) in order to make the equation explicitly second kind. In the process of numerically validating the $2d$ PBI, however, we found a simpler algorithm that accurately evaluates the required double integral operators in much less time. In contrast to previously implemented methods, the spectrum of the discretized operator produced by this method faithfully

reproduces that of the continuous operator even for high spatial frequency eigenmodes.

One of the surprising outcomes of this program is the observation that, for certain open surface PEC targets, the spectrum of the analytically preconditioned EFIE (APEFIE) includes one or two zero eigenvalues. We endeavored to analytically derive the spectrum of the APEFIE on a PEC disk to determine the source of the zero eigenvalues, but were unable to obtain definitive results before the conclusion of the program. Nonetheless, our report contains a summary of the analytical results we did obtain for open surface scattering from canonical targets in the $2d$ and $3d$ scalar/acoustic cases and the $3d$ vector/EM case.

2 Introduction

The electric field integral equation (EFIE) is an essential element in the arsenal of tools for doing frequency domain electromagnetic scattering calculations. It is the only integral equation that can be applied to both open and closed surface PEC targets

The EFIE has a serious problem, however – it is notoriously ill conditioned. When the system of linear equations generated by the EFIE is solved by an iterative method, the iteration count cannot be controlled. This compromises the effectiveness of acceleration methods such as the fast multipole method (FMM) because such methods necessarily rely on iterative solvers. Even when a direct solver (e.g., LU decomposition) can be used, the combination of a seriously ill conditioned linear system and finite precision computer arithmetic can degrade the accuracy of the computed solution.

The goal of this program is to find an analytic preconditioner for the EFIE that

- converts the EFIE to a second kind integral operator,
- applies to both open and closed surface PEC targets, and
- is amenable to efficient numerical implementation.

Our approach is based on two observations.

The first is the EFIE preconditioning method described in [1]. When applied to closed surface scattering problems, this analytic preconditioner is guaranteed to convert the EFIE to a second kind integral equation. The computational cost of this approach is predictable and reasonable. However,

our original implementation of this approach did not produce a second kind integral equation when applied to an open surface scatterer.

The second observation is a $2d$ extension [2][3] of a well established, but not so widely known, $1d$ integral identity called the Poincaré-Bertrand identity (PBI) [4]. Analytic preconditioners for the $2d$ and $3d$ scalar analogs of the EFIE produce double integral operators that exhibit second kind behavior. However, the second kind behavior may be lost as a result of numerical discretization. The $1d$ and $2d$ Poincaré-Bertrand identities provide a way to write these double integral operators in an explicitly second kind form, i.e., as the sum of a constant term and a compact operator, which makes it trivial to retain second kind behavior in the numerical implementation. Furthermore, the Poincaré-Bertrand identities can be used both with open and closed surface formulations.

Work on the program was divided into three tasks:

1. Numerically validate the $2d$ PBI on simple $2d$ surfaces.

2. Use the $2d$ PBI to realize an explicitly second kind analytically preconditioned EFIE (APEFIE) for closed surface PEC targets.

3. Use the $2d$ PBI to realize an explicitly second kind APEFIE for open surface PEC targets.

We completed all three tasks and achieved the stated objectives. In the course of our work, however, we found a faster, more robust alternative to the $2d$ PBI for achieving second kind behavior in a numerical realization of the APEFIE. The alternative method involves overdiscretizing the double integral evaluations at intermediate sample points. An intermediate sample point density about double that of the field/source point discretization was generally sufficient to avoid compromising accuracy. We used this alternative method in our numerical demonstrations.

Notes:

- EFIE ill conditioning has a local cause and a global cause. This program is only concerned with addressing the local cause. It does not directly address resonances, whether spurious or physical, which fall into the global cause category.

- The primary motivation for developing a well conditioned counterpart to the EFIE is to facilitate the use of fast methods such as the FMM for solving large scattering problems involving open PEC surfaces.

The goal of this program was limited to finding a suitable integral equation formulation and demonstrating its potential on small scale, open surface scattering problems. Since the underlying cause of the problem is a local one, the methods reported here should be just as effective on large scale scattering problems as they were for the small test targets investigated here.

We believe that this new formulation can have far-reaching impact because it removes a major impediment to the practical use of fast methods for solving a wide variety of important scattering problems. The types of problems that would be affected range from predicting the radar cross section (RCS) of airborne vehicles with thin fins or antennas to modeling microwave circuits comprising thin strips of metallization on multi-layer substrates. Note that the new formulation also applies to $3d$ scalar scattering so it can be used to improve solution methods for acoustic scattering problems as well.

3 Poincaré-Bertrand Identity

The Poincaré-Bertrand identities (PBI) [3][4] provide a means to explicitly second kind expressions for the double integral operators that arise when analytic preconditioning methods are applied to the $2d$ and $3d$ scalar scattering analogs of the EFIE. Although we ended up not using these identities in our formulation of a well conditioned EFIE for open and closed surfaces, a brief discussion of the relevant identities is include here for completeness.

3.1 $2d$ scalar

The Poincaré-Bertrand identity is commonly stated as[1]

$$\begin{aligned} &\fint_{-1}^{1} dx' \frac{\phi_1(x')}{x-x'} \fint_{-1}^{1} dx'' \frac{\phi_2(x'')}{x'-x''} \psi(x'') = -\pi^2 \phi_1(x)\, \phi_2(x)\, \psi(x) \\ &+ \fint_{-1}^{1} dx'' \phi_2(x'') \fint_{-1}^{1} dx' \frac{\phi_1(x')}{(x-x')(x'-x'')} \psi(x'') \end{aligned} \tag{1}$$

where $\fint$ means that the integral is a Cauchy principal value integral. Equation (1) expresses the $1d$ PBI on the open interval $(-1, 1)$. A more general

[1]The redundant function $\psi(x'')$ is given separately from $\phi_2(x'')$ for later notational convenience. It will correspond to the unknown source function.

form of the $1d$ PBI is

$$\begin{aligned}
&\oint_C dl' \phi_1\left(\mathbf{x}'\right) \frac{\partial G\left(\mathbf{x}, \mathbf{x}'\right)}{dl'} \oint_C dl'' \phi_2\left(\mathbf{x}''\right) \frac{\partial G\left(\mathbf{x}', \mathbf{x}''\right)}{dl''} \psi\left(\mathbf{x}''\right) = \\
&-\frac{1}{4} \phi_1(\mathbf{x}) \phi_2(\mathbf{x}) \psi(\mathbf{x}) \\
&+\oint_C dl'' \phi_2\left(\mathbf{x}''\right) \oint_C dl' \phi_1\left(\mathbf{x}'\right) \frac{\partial G\left(\mathbf{x}, \mathbf{x}'\right)}{dl'} \frac{\partial G\left(\mathbf{x}', \mathbf{x}''\right)}{dl''} \psi\left(\mathbf{x}''\right)
\end{aligned} \tag{2}$$

where the integrals are now over arc length on an arbitrary smooth curve C, the derivatives are tangential (to C) derivatives, and G is the $2d$ Laplace or Helmholtz kernel, i.e.,

$$G\left(\mathbf{x}, \mathbf{x}'\right) = -\frac{1}{2\pi} \log\left(\left|\mathbf{x}-\mathbf{x}'\right|\right) \quad \text{or} \quad G\left(\mathbf{x}, \mathbf{x}'\right) = \frac{i}{4} H_0^{(1)}\left(\left|\mathbf{x}-\mathbf{x}'\right|\right), \tag{3}$$

respectively.

The $2d$ analogs of the EFIE are a first kind integral equation

$$\psi^{inc}(\mathbf{x}) = \int_C dl' G\left(\mathbf{x}, \mathbf{x}'\right) \frac{d\psi\left(\mathbf{x}'\right)}{dn'} \qquad \text{for TM polarization} \tag{4}$$

and a hypersingular integral equation

$$\frac{d\psi^{inc}(\mathbf{x})}{dn} = -\frac{d}{dn} \int_C dl' \frac{\partial G\left(\mathbf{x}, \mathbf{x}'\right)}{\partial n'} \psi\left(\mathbf{x}'\right) \qquad \text{for TE polarization} \tag{5}$$

where the derivatives are normal (to C) derivatives.

If curve C is closed, one obtains a second kind integral equation from (4) or (5) by pre- or post-conditioning it by the integral operator of the other equation [5][6]. The resulting composite operator can be manipulated into a sum of terms involving compact operators, plus a term whose form matches that of the LHS of (2) with $\phi_1\left(\mathbf{x}'\right) = \phi_2\left(\mathbf{x}''\right) = 1$. This term has the spectral characteristics of a second kind operator. Using (2), we can write it in an explicitly second kind form.

If C is an open curve, one can apply the same procedure to obtain second kind integral equations, provided additional factors containing the appropriate endpoint singularity behavior are included in each integral operator [7][8]. In the case of the open interval $(-1, 1)$, this amounts to letting

$$\phi_1\left(x'\right) = \left(1-\left(x'\right)^2\right)^{\pm 1/2} \quad \text{and} \quad \phi_2\left(x''\right) = \left(1-\left(x''\right)^2\right)^{\mp 1/2}. \tag{6}$$

Since $\phi_1(x)\,\phi_2(x) = 1$ in both cases, the transformation of (2) again produces an explicitly second kind integral operator.

Notes:

- Having an explicitly second kind EFIE formulation for $2d$ scattering is helpful because it makes solution methods based on patch-based discretizations practical, but it is not essential because in $2d$ an entire-domain discretization based on arc length is often available.

- The form of the $1d$ PBI suggests a possible means to obtain a second kind integral equation for a target with both open and closed characteristics. Consider, for example, a circle with a thin fin attached. It may be possible to obtain a second kind formulation for this geometry by choosing $\phi_2(\mathbf{x})$ to be a function that incorporates the appropriate endpoint singularity behavior at the open end of the fin and smoothly approaches unity at the other end of the fin, and by choosing $\phi_1(x)$ to incorporate the reciprocal behavior.

- The PBI is needed for computational purposes only when the field and source points are in close proximity. Most interactions are far interactions and they can be computed using standard discretizations of the integral operators or using fast methods such as the FMM.

3.2 $3d$ scalar

We can write the $2d$ extension to the $1d$ PBI [2][3] as

$$\begin{aligned}
&\int_S ds' \phi_1(\mathbf{x}') \nabla' G(\mathbf{x}, \mathbf{x}') \cdot \int_S ds'' \phi_2(\mathbf{x}'') \nabla' G(\mathbf{x}', \mathbf{x}'') \psi(\mathbf{x}'') \\
&= \frac{1}{4} \phi_1(\mathbf{x}) \phi_2(\mathbf{x}) \psi(\mathbf{x}) + \\
&\int_S ds'' \phi_2(\mathbf{x}'') \int_S ds' \phi_1(\mathbf{x}') \nabla' G(\mathbf{x}, \mathbf{x}') \cdot \nabla' G(\mathbf{x}', \mathbf{x}'') \psi(\mathbf{x}'')
\end{aligned} \tag{7}$$

where the integrations are over a sufficiently smooth surface S and $\nabla' G$ denotes the gradient of the $3d$ Laplace kernel with respect to $\mathbf{x}'$. The extension of (7) to the case of the $3d$ Helmholtz kernel is trivial.

The equations for scalar scattering from a surface S under Dirichlet and Neumann boundary conditions are analogous to (4) and (5), respectively. The procedures for pre- or post-conditioning these equations to obtain second kind integral equations are also analogous to those of the $2d$ scalar case.

4 Analytically preconditioning the EFIE

The electric field integral equation (EFIE) for a PEC is

$$-\widehat{\mathbf{n}}\left(\mathbf{x}\right)\times\mathbf{E}^{inc}\left(\mathbf{x}\right)=\overbrace{\widehat{\mathbf{n}}\left(\mathbf{x}\right)\times\int_{S}ds'\left\{ikG\left(\mathbf{x},\mathbf{x}'\right)\mathbf{J}\left(\mathbf{x}'\right)+\frac{i}{k}\nabla\left(\nabla G\left(\mathbf{x},\mathbf{x}'\right)\cdot\mathbf{J}\left(\mathbf{x}'\right)\right)\right\}}^{T\mathbf{J}}, \tag{8}$$

where $\widehat{\mathbf{n}}\left(\mathbf{x}\right)$ is the unit normal at the field point $\mathbf{x}$, $\mathbf{E}^{inc}\left(\mathbf{x}\right)$ is the incident electric field, $k=\sqrt{\mu\epsilon}\omega$ is the propagation wavenumber in the interaction medium, $G\left(\mathbf{x},\mathbf{x}'\right)$ is the Helmholtz kernel, and $\mathbf{J}\left(\mathbf{x}'\right)$ is the equivalent surface source distribution (or current). The current is related to the surface component of the magnetic field $\mathbf{H}$ by $\mathbf{J}=Z\widehat{\mathbf{n}}\times\mathbf{H}$, where $Z=\sqrt{\mu/\epsilon}$ is the wave impedance in the interaction medium.

The ill conditioned nature of the EFIE is a direct result of the near field behavior of the EFIE integral operator, which we can write as the sum of singular and hypersingular component operators:

$$T^{S}=ik\widehat{\mathbf{n}}\left(\mathbf{x}\right)\times\int_{S}ds'\;G\left(\mathbf{x},\mathbf{x}'\right) \tag{9}$$

$$T^{H}=\frac{i}{k}\widehat{\mathbf{n}}\left(\mathbf{x}\right)\times\nabla\int_{S}ds'\;\nabla G\left(\mathbf{x},\mathbf{x}'\right)\cdot \tag{10}$$

The singular component T^S is a smoothing operator – eigenvalues of T^S corresponding to high spatial frequency eigenmodes tend toward the origin. The hypersingular component T^H is a differential operator – eigenvalues of T^H corresponding to high spatial frequency eigenmodes tend toward infinity. Note that T^S is the $3d$ EM analog of the TM operator on the RHS of (4) and T^H is the $3d$ EM analog of the TE operator in (5). The EFIE combines both sources of ill conditioning into a single integral equation, adding to the challenge of finding a suitable analytic preconditioner for open surface targets.

4.1 Original analytic preconditioner

As described in [1], the ideal preconditioner for the EFIE for closed surface targets is the EFIE operator itself. In other words, $T^2\equiv TT$ is a second kind operator. At first glance, this may seem surprising since the expanded

product operator contains a double hypersingular term:

$$\begin{aligned} T^2\mathbf{J} &= \left(T^S + T^H\right)\left(T^S + T^H\right)\mathbf{J} \\ &= \left(T^S T^S + T^H T^S + T^S T^H + T^H T^H\right)\mathbf{J}. \end{aligned} \tag{11}$$

However, integration by parts reveals that the double hypersingular term actually vanishes

$$\begin{aligned} T^H T^H \mathbf{J} &= (\widehat{\mathbf{n}} \times \nabla) \int_S ds' \; \nabla G \cdot \left(\widehat{\mathbf{n}}' \times \nabla'\right) \int_S ds'' \; \nabla' G \cdot \mathbf{J}'' \\ &= (\widehat{\mathbf{n}} \times \nabla) \int_S ds' \; G \underbrace{\nabla' \cdot \left(\widehat{\mathbf{n}}' \times \nabla'\right)}_{=\,0} \int_S ds'' \; \nabla' G \cdot \mathbf{J}'' = 0, \end{aligned} \tag{12}$$

which leaves

$$T^2\mathbf{J} = \left(T^H T^S + T^S T^H + T^S T^S\right)\mathbf{J} \tag{13}$$

The combination of the first two terms on the RHS of (13) is a second kind operator. The last term is obviously compact. With some further manipulation (see [1]), we can re-write (13) as

$$\begin{aligned} T^2\mathbf{J} =& \overbrace{\widehat{\mathbf{n}} \times \int_S ds' \; \nabla G\left(\mathbf{x}, \mathbf{x}'\right)}^{T^\alpha} \overbrace{\int_S ds'' \left(\widehat{\mathbf{n}}' \times \nabla' G\left(\mathbf{x}', \mathbf{x}''\right)\right) \cdot \mathbf{J}\left(\mathbf{x}''\right)}^{T^T} \\ &+ \overbrace{\widehat{\mathbf{n}} \times \int_S ds' \; \widehat{\mathbf{n}}' \times \nabla' G\left(\mathbf{x}, \mathbf{x}'\right)}^{T^\beta} \overbrace{\int_S ds'' \; \nabla' G\left(\mathbf{x}', \mathbf{x}''\right) \cdot \mathbf{J}\left(\mathbf{x}''\right)}^{T^L} \\ &- k^2 \overbrace{\widehat{\mathbf{n}} \times \int_S ds' \; G\left(\mathbf{x}, \mathbf{x}'\right) \widehat{\mathbf{n}}'}^{T^S/(ik)} \times \overbrace{\int_S ds'' \; G\left(\mathbf{x}', \mathbf{x}''\right) \mathbf{J}\left(\mathbf{x}''\right)}^{T^S/(ik)}, \end{aligned} \tag{14}$$

which has the appealing property that the kernel of each integral operator involves no more than one gradient on the Green function.

The surface current $\mathbf{J}$ can be decomposed[2] into two parts, a transverse part $\mathbf{J}^T$ that has no surface divergence ($\nabla \cdot \mathbf{J}^T = 0$) and a longitudinal component $\mathbf{J}^L$ that has no surface curl ($(\widehat{\mathbf{n}} \times \nabla) \cdot \mathbf{J}^L = 0$). One can show

[2] According to the Helmholtz-Hodge decomposition theorem [9], a surface vector field can be decomposed into a curl-free component, a divergence-free component, and a harmonic remainder (which is both curl- and divergence-free). When it exists, the harmonic component of $\mathbf{J}$ needs to be treated separately.

analytically [1] that $T^H T^S$ (or $T^\alpha T^T$) is a second kind operator for $\mathbf{J}^T$ and is compact for $\mathbf{J}^L$. Conversely, $T^S T^H$ (or $T^\beta T^L$) is a second kind operator for $\mathbf{J}^L$ and is compact for $\mathbf{J}^T$. Therefore the sum $T^H T^S + T^S T^H$ (or $T^\alpha T^T + T^\beta T^L$) is a second kind operator for the full current $\mathbf{J} = \mathbf{J}^T + \mathbf{J}^L$.

4.2 Eigenvalues and resonances

The magnetic field integral equation (MFIE),

$$\widehat{\mathbf{n}}(\mathbf{x}) \times \mathbf{H}^{inc}(\mathbf{x}) = \frac{1}{2}\mathbf{J}(\mathbf{x}) \underbrace{-\widehat{\mathbf{n}}(\mathbf{x}) \times \nabla \int_S ds'\, G(\mathbf{x}, \mathbf{x}')}_{K} \mathbf{J}(\mathbf{x}'), \tag{15}$$

only applies to closed surface targets.

If S is a closed surface, the T^2 operator obeys the following identity from Roach [10]:

$$T^2 = -\frac{1}{4} + K^2 = \left(-\frac{1}{2} + K\right)\left(\frac{1}{2} + K\right). \tag{16}$$

Since K is compact, the Roach identity confirms that T^2 is a second kind operator whose eigenvalues accumulate at $-\frac{1}{4}$.

The factored representation of T^2 in (16) shows that resonances of $\frac{1}{2}+K$ and $-\frac{1}{2}+K$ are also resonances of T^2. So even though preconditioning both sides of (8) turns it into a second kind integral equation, it does not, by itself, always produce a well conditioned integral equation. There are a number of simple and effective ways (e.g., see [1][11]) to eliminate these spurious resonances without compromising the effectiveness of the analytic preconditioner.

Part of the solution to avoiding spurious resonances is to use a different wavenumber for the preconditioning operator. For example, if $k_2 = k$ is the wavenumber of the scattering problem, one can use $k_1 = ik$ for the preconditioning operator. As we saw in our previous work [1], the resultant integral operator $T(k_1)\,T(k_2)$ is no longer a single second kind operator, but rather the sum of two second kind operators with different asymptotic collection point, one at $+\frac{i}{2}$ and another at $-\frac{i}{2}$. In the course of this program we realized that a simple modification to the preconditioning procedure puts both asymptotic collection points back at $-\frac{1}{4}$.

The sum of $T(k_2)$ preconditioned by $\alpha^S T^S(k_1)$ and $T(k_2)$ preconditioned by $\alpha^H T^H(k_1)$, where α^S and α^H are arbitrary coefficients, can be rewritten as

$$\alpha^H \frac{k_2}{k_1} T^\alpha(k_1)\,T^T(k_2) + \alpha^S \frac{k_1}{k_2} T^\beta(k_1)\,T^L(k_2) - \alpha^S T^S(k_1)\,T^S(k_2). \tag{17}$$

Setting $\alpha^S = \alpha^H = 1$ produces the same result as before. On the other hand, setting

$$\alpha^H = \frac{k_1}{k_2} \quad \text{and} \quad \alpha^S = \frac{k_2}{k_1}$$

puts both eigenvalue collections points at $-\frac{1}{4}$, independently of the values of k_1 and k_2. Having a single asymptotic eigenvalue collection point improves iterative solver convergence.

5 Numerical validation of $2d$ PBI

The $2d$ Poincaré-Bertrand identity (PBI) can be written as

$$\begin{aligned}
&\int_S ds'\ \phi_1\left(\mathbf{x}'\right)\left(\widehat{\mathbf{n}} \times \nabla G\left(\mathbf{x}, \mathbf{x}'\right)\right) \cdot \int_S ds''\ \phi_2\left(\mathbf{x}''\right)\left(\widehat{\mathbf{n}}'' \times \nabla'' G\left(\mathbf{x}', \mathbf{x}''\right)\right) \psi\left(\mathbf{x}''\right) \\
&= \frac{1}{4}\phi_1\left(\mathbf{x}\right)\phi_2\left(\mathbf{x}\right)\psi\left(\mathbf{x}\right) + \qquad (18) \\
&\int_S ds''\ \phi_2\left(\mathbf{x}''\right)\psi\left(\mathbf{x}''\right) \int_S ds'\ \phi_1\left(\mathbf{x}'\right)\left(\widehat{\mathbf{n}} \times \nabla G\left(\mathbf{x}, \mathbf{x}'\right)\right) \cdot \left(\widehat{\mathbf{n}}'' \times \nabla'' G\left(\mathbf{x}', \mathbf{x}''\right)\right)
\end{aligned}$$

where S is a smooth surface (open or closed), ϕ_1, ϕ_2, and ψ are general smooth functions, and G is the $3d$ Laplace kernel (i.e., $G\left(\mathbf{x}, \mathbf{x}'\right) = 1/\left(4\pi r\right)$, where $r \equiv |\mathbf{x} - \mathbf{x}'|$). The identity expresses the fact that the two integral operators

$$H_1 \equiv \int_S ds'\ \phi_1\left(\mathbf{x}'\right)\left(\widehat{\mathbf{n}} \times \nabla G\left(\mathbf{x}, \mathbf{x}'\right)\right) \cdot \qquad (19a)$$

$$H_2 \equiv \int_S ds''\ \phi_2\left(\mathbf{x}''\right)\left(\widehat{\mathbf{n}}'' \times \nabla'' G\left(\mathbf{x}', \mathbf{x}''\right)\right) \qquad (19b)$$

do not commute. Instead, the commutator is

$$[H_1, H_2] = \frac{1}{4}\phi_1\left(\mathbf{x}\right)\phi_2\left(\mathbf{x}\right).$$

The identity also holds for the Helmholtz kernel (i.e., $G\left(\mathbf{x}, \mathbf{x}'\right) = e^{ikr}/\left(4\pi r\right)$) since the Helmholtz kernel can be decomposed into the sum of a singular (Laplace) part and a regular part and for the regular part the operators do commute.

The first objective of this contract was to numerically demonstrate the validity of this identity in the restricted case where $\phi_1 = \phi_2 = 1$ and $G\left(\mathbf{x}, \mathbf{x}'\right)$

is the $3d$ Laplace kernel, i.e.,

$$\int_S ds' \ \left(\widehat{\mathbf{n}} \times \nabla G\left(\mathbf{x}, \mathbf{x}'\right)\right) \cdot \int_S ds'' \ \left(\widehat{\mathbf{n}}'' \times \nabla'' G\left(\mathbf{x}', \mathbf{x}''\right)\right) \psi\left(\mathbf{x}''\right)$$
$$= \frac{1}{4}\psi\left(\mathbf{x}\right) +$$
$$\int_S ds'' \ \psi\left(\mathbf{x}''\right) \int_S ds' \ \left(\widehat{\mathbf{n}} \times \nabla G\left(\mathbf{x}, \mathbf{x}'\right)\right) \cdot \left(\widehat{\mathbf{n}}'' \times \nabla'' G\left(\mathbf{x}', \mathbf{x}''\right)\right),$$

or

$$I_{DHT} \ \psi\left(\mathbf{x}\right) = \frac{1}{4}\psi\left(\mathbf{x}\right) + I_{PBI} \ \psi\left(\mathbf{x}\right),$$

where I_{DHT} and I_{PBI} represent the double integral operators, defined by

$$I_{DHT} \ \psi\left(\mathbf{x}\right) \equiv \int_S ds' \ \left(\widehat{\mathbf{n}} \times \nabla G\left(\mathbf{x}, \mathbf{x}'\right)\right) \cdot \int_S ds'' \ \left(\widehat{\mathbf{n}}'' \times \nabla'' G\left(\mathbf{x}', \mathbf{x}''\right)\right) \psi\left(\mathbf{x}''\right) \tag{20a}$$

$$I_{PBI} \ \psi\left(\mathbf{x}\right) \equiv \int_S ds'' \ \psi\left(\mathbf{x}''\right) \int_S ds' \ \left(\widehat{\mathbf{n}} \times \nabla G\left(\mathbf{x}, \mathbf{x}'\right)\right) \cdot \left(\widehat{\mathbf{n}}'' \times \nabla'' G\left(\mathbf{x}', \mathbf{x}''\right)\right). \tag{20b}$$

We developed prototype code in C++ that evaluates each of these terms and demonstrates the validity of this identity on several types of surface patches.

5.1 Integral operator properties

We can consider the validation procedure as involving the evaluation of four different integrals:

$$I_1\left(\mathbf{x}\right) \equiv \int_S ds' \ \left(\widehat{\mathbf{n}} \times \nabla G\left(\mathbf{x}, \mathbf{x}'\right)\right) \cdot \mathbf{f}\left(\mathbf{x}'\right)$$
$$\mathbf{I}_2\left(\mathbf{x}'\right) \equiv \int_S ds'' \ \left(\widehat{\mathbf{n}}'' \times \nabla'' G\left(\mathbf{x}', \mathbf{x}''\right)\right) f\left(\mathbf{x}''\right)$$
$$I_3\left(\mathbf{x}\right) \equiv \int_S ds'' \ I_4\left(\mathbf{x}, \mathbf{x}''\right) f\left(\mathbf{x}''\right)$$
$$I_4\left(\mathbf{x}, \mathbf{x}''\right) \equiv \int_S ds' \ \left(\widehat{\mathbf{n}} \times \nabla G\left(\mathbf{x}, \mathbf{x}'\right)\right) \cdot \left(\widehat{\mathbf{n}}'' \times \nabla'' G\left(\mathbf{x}', \mathbf{x}''\right)\right)$$

where $f\left(\mathbf{x}''\right)$ is an arbitrary scalar function (which one could later use to represent the unknown source distribution) and $\mathbf{f}\left(\mathbf{x}'\right)$ is an arbitrary surface

vector function. The combination of I_1 and $\mathbf{I}_2$ gives I_{DHT} and the combination of I_3 and I_4 gives I_{PBI}. The four integrals involve different types of kernel singularities and must be handled carefully to achieve accurate, numerically realizable results.

Our prototype code evaluates the double Hilbert transform integral $I_{DHT}\, f(\mathbf{x}'')$ by multiplying the separate matrix representations (i.e., discretized versions) of $I_1(\mathbf{x})$ and $\mathbf{I}_2(\mathbf{x}')$. By contrast, we evaluate the double integral $I_{PBI}\, f(\mathbf{x}'')$ "all at once" using numerical evaluations of the inner integral $I_4(\mathbf{x}, \mathbf{x}'')$ at each quadrature point of the outer integral $I_3(\mathbf{x})$. The "all at once" integration procedure is more time consuming, but is also more reliable for computing accurate results.

We have observed the following properties:

- The kernels of I_1 and $\mathbf{I}_2$ have singularities that scale as $\cos(\theta)\, r^{-2}$ (where r is the distance from the source point to the field point and θ measures the angle around the field point) so they are integrable, but only in the principal value sense. This requires some care. For example, one can rewrite each integral using integration by parts as the sum of a edge integral of a regular function and a surface integral of a function whose kernel singularity is no worse than r^{-1}.

- $I_1(\mathbf{x})$ is a smooth function of $\mathbf{x}$ for $\mathbf{x} \in S$. For $\mathbf{x}$ near an open edge of S, $I_1(\mathbf{x})$ varies as $\log(r)$ where r is the distance from $\mathbf{x}$ to the open edge. $\mathbf{I}_2(\mathbf{x}')$ behaves similarly.

- The integrand of $I_4(\mathbf{x}, \mathbf{x}'')$ is singular at $\mathbf{x}$ and $\mathbf{x}''$. Each singularity scales like $\cos(\theta)\, r^{-2}$, where r is the distance from the source point to the singular point and θ measures the angle around the singular point. As with I_1 and $\mathbf{I}_2$, they are integrable singularities in the principal value sense because of the angular factor. When $\mathbf{x}$ and $\mathbf{x}''$ are close together special care must be taken to evaluate the integral accurately because the integrand varies rapidly between positive and negative infinities. We have investigated several approaches to evaluating this integral, including some that involve analytic singularity subtraction. They all work, but with varying degrees of efficiency and robustness.

- On a flat surface, $I_4(\mathbf{x}, \mathbf{x}'')$ is a smooth function of $\mathbf{x}''$ for a given $\mathbf{x}$, even at $\mathbf{x} = \mathbf{x}''$. If S is curved, then $I_4(\mathbf{x}, \mathbf{x}'')$ has a $\log(r)$ singularity, where $r \equiv |\mathbf{x} - \mathbf{x}''|$. For $\mathbf{x}''$ near an open edge of S, $I_4(\mathbf{x}, \mathbf{x}'')$ varies as $\log(r)$ where r is the distance from $\mathbf{x}''$ to the open edge.

- In one sense $I_3(\mathbf{x})$ is the easiest of the integrals to evaluate since the singularities of its kernel $I_4(\mathbf{x}, \mathbf{x}'')$ are no worse that $\log(r)$. However, it can be the most time consuming to evaluate because at each quadrature point one needs an accurate evaluation of $I_4(\mathbf{x}, \mathbf{x}'')$.

5.2 Numerical results

Our prototype code can evaluate $I_{DHT}\ f(\mathbf{x})$ and $I_{PBI}\ f(\mathbf{x})$ with adjustable accuracy on a variety of patch types with a variety of testing functions. The computation takes a 'digits' parameter, which specifies the accuracy goal (in number of digits) of the adaptive integration routines. For $I_{DHT}\ f(\mathbf{x})$, there is also an 'order' parameter. It specifies the number of $\mathbf{x}'$ points at which $\mathbf{I}_2(\mathbf{x}')$ is evaluated, which is also the number of testing functions $\mathbf{f}(\mathbf{x}')$ used to compute local corrections for $I_1(\mathbf{x})$.

The testing functions we chose are products of polynomials in the surface parameterization u_1 and u_2. The tables below are organized such that the entry in the m^{th} row and n^{th} column corresponds to the scalar function

$$f(\mathbf{x}'') = f(u_1, u_2) = P_m(u_1) P_n(u_2)$$

where $P_n(u)$ is the n^{th} Legendre polynomial.

For easy comparison, the tables show computed values of $\left(I_{DHT} - \frac{1}{4}\right) f(\mathbf{x})$ and $I_{PBI}\ f(\mathbf{x})$.

5.2.1 Square patch

Tables 1 and 2 give $\left(I_{DHT} - \frac{1}{4}\right) f(\mathbf{x})$ and Tables 3 and 4 give $I_{PBI}\ f(\mathbf{x})$ on a square patch at $\mathbf{x} = (0.25, 0.35)$. Table 5 gives the difference between $\left(I_{DHT} - \frac{1}{4}\right) f(\mathbf{x})$ (from Table 2) and $I_{PBI}\ f(\mathbf{x})$ (from Table 4).

Table 1: $\left(I_{DHT} - \frac{1}{4}\right) f(x)$ for a square patch (digits=10 and order=8)

m/n	0	1	2	3	4
0	-0.10514744	0.02500997	-0.00878341	-0.00051174	-0.01157399
1	0.03965702	-0.01959232	-0.00205752	0.00387275	0.00661861
2	-0.02384387	0.00801955	0.01640285	-0.00927404	0.00050915
3	0.00873452	-0.00266640	-0.01145919	0.00844339	-0.00138054
4	-0.01365415	0.00459554	0.00706801	-0.00530567	0.00024560

Table 2: $\left(I_{DHT} - \frac{1}{4}\right) f(x)$ for a square patch (digits=10 and order=10)

m/n	0	1	2	3	4
0	-0.10517396	0.02501531	-0.00882176	-0.00052061	-0.01164151
1	0.03968532	-0.01959947	-0.00199779	0.00391992	0.00678708
2	-0.02383721	0.00800491	0.01638150	-0.00929691	0.00045280
3	0.00878461	-0.00267033	-0.01135429	0.00839380	-0.00129506
4	-0.01365726	0.00464442	0.00699183	-0.00547012	0.00012730

Table 3: $I_{PBI}\ f(x)$ for a square patch (digits=6)

m/n	0	1	2	3	4
0	-0.10515237	0.02500882	-0.00879625	-0.00052500	-0.01162961
1	0.03967821	-0.01960292	-0.00200786	0.00388514	0.00675064
2	-0.02385828	0.00801653	0.01636798	-0.00930678	0.00043937
3	0.00879925	-0.00272262	-0.01136585	0.00844514	-0.00131449
4	-0.01368469	0.00462558	0.00704841	-0.00545916	0.00016687

Table 4: $I_{PBI}\ f(x)$ for a square patch (digits=8)

m/n	0	1	2	3	4
0	-0.10515263	0.02500873	-0.00879683	-0.00052512	-0.01163036
1	0.03967805	-0.01960298	-0.00200822	0.00388503	0.00675015
2	-0.02385886	0.00801634	0.01636670	-0.00930704	0.00043773
3	0.00879902	-0.00272271	-0.01136637	0.00844499	-0.00131519
4	-0.01368545	0.00462536	0.00704675	-0.00545947	0.00016474

Table 5: $\left(I_{DHT}\ -\frac{1}{4}\right) f(x) - I_{PBI}\ f(x)$ for a square patch

m/n	0	1	2	3	4
0	-0.00002133	0.00000658	-0.00002493	0.00000451	-0.00001115
1	0.00000727	0.00000351	0.00001043	0.00003489	0.00003693
2	0.00002165	-0.00001143	0.00001480	0.00001013	0.00001507
3	-0.00001441	0.00005238	0.00001208	-0.00005119	0.00002013
4	0.00002819	0.00001906	-0.00005492	-0.00001065	-0.00003744

5.2.2 Ogive patch

Tables 6 and 7 give $\left(I_{DHT} - \frac{1}{4}\right) f(\mathbf{x})$ and Tables 8 and 9 give $I_{PBI}\ f(\mathbf{x})$ on an ogive patch at $\mathbf{x} = (0.25, 0.35)$. Table 10 gives the difference between $\left(I_{DHT} - \frac{1}{4}\right) f(\mathbf{x})$ (from Table 7) and $I_{PBI}\ f(\mathbf{x})$ (from Table 9).

Table 6: $\left(I_{DHT} - \frac{1}{4}\right) f(x)$ for an ogive patch (digits=10 and order=8)

m/n	0	1	2	3	4
0	-0.10497214	0.01531734	-0.00434583	0.00114802	-0.01055496
1	0.02877761	-0.00922837	-0.00005219	0.00023867	0.00550509
2	-0.01299734	0.00165363	0.01443126	-0.00469695	-0.00057568
3	0.00033876	0.00098081	-0.00769284	0.00398050	-0.00029916
4	-0.01035685	0.00215251	0.00574442	-0.00231159	-0.00099865

Table 7: $\left(I_{DHT} - \frac{1}{4}\right) f(x)$ for an ogive patch (digits=10 and order=10)

m/n	0	1	2	3	4
0	-0.10496593	0.01530208	-0.00434915	0.00108919	-0.01056134
1	0.02877142	-0.00924484	-0.00001177	0.00045047	0.00550813
2	-0.01300874	0.00168139	0.01440599	-0.00460083	-0.00046958
3	0.00032182	0.00092830	-0.00763120	0.00357058	-0.00050284
4	-0.01027579	0.00219966	0.00561910	-0.00213368	-0.00077999

Table 8: $I_{PBI}\ f(x)$ for an ogive patch (digits=6)

m/n	0	1	2	3	4
0	-0.10469727	0.01519943	-0.00457952	0.00114313	-0.01047368
1	0.02852133	-0.00909148	0.00027490	0.00028032	0.00536309
2	-0.01319548	0.00178295	0.01468790	-0.00468231	-0.00059081
3	0.00047419	0.00080978	-0.00791684	0.00375302	-0.00029897
4	-0.01027494	0.00217714	0.00564040	-0.00215186	-0.00082333

Table 9: $I_{PBI}\ f(x)$ for an ogive patch (digits=8)

m/n	0	1	2	3	4
0	-0.10469748	0.01519944	-0.00457999	0.00114316	-0.01047425
1	0.02852126	-0.00909165	0.00027474	0.00028003	0.00536283
2	-0.01319595	0.00178299	0.01468690	-0.00468222	-0.00059207
3	0.00047410	0.00080952	-0.00791710	0.00375258	-0.00029937
4	-0.01027553	0.00217723	0.00563913	-0.00215167	-0.00082491

Table 10: $\left(I_{DHT}\ -\frac{1}{4}\right) f(x) - I_{PBI}\ f(x)$ for an ogive patch

m/n	0	1	2	3	4
0	-0.00026845	0.00010264	0.00023084	-0.00005397	-0.00008709
1	0.00025016	-0.00015319	-0.00028651	0.00017044	0.00014530
2	0.00018721	-0.00010160	-0.00028091	0.00008139	0.00012249
3	-0.00015228	0.00011878	0.00028590	-0.00018200	-0.00020347
4	-0.00000026	0.00002243	-0.00002003	0.00001799	0.00004492

5.3 Discussion

As the 'digits' parameter increases, the computed value of $I_{PBI}\ f(\mathbf{x})$ converges for each scalar function. Likewise, as the 'order' parameter increases, the computed value of $I_{DHT}\ f(\mathbf{x})$ converges for each scalar function.

The computed values of $I_{PBI}\ f(\mathbf{x})$ generally show faster convergence than those of $I_{DHT}\ f(\mathbf{x})$, which is a direct consequence of the fact that we are using a two stage approach to computing $I_{DHT}\ f(\mathbf{x})$, rather than the all-at-once approach used to compute $I_{PBI}\ f(\mathbf{x})$. If we were to compute $I_{DHT}\ f(\mathbf{x})$ using double adaptive integration, as we do to compute $I_{PBI}\ f(\mathbf{x})$, the convergence rate would be similar.

In any case, $\left(I_{DHT}\ -\frac{1}{4}\right) f(\mathbf{x})$ and $I_{PBI}\ f(\mathbf{x})$ converge to approximately the same value for each patch. Table 5 shows that for the square patch the difference is less than 6×10^{-5} for all 25 scalar functions and Table 10 shows that for the ogive patch the difference is less than 3×10^{-4} for all 25 scalar functions.

Although this does not constitute a proof that the $2d$ PBI identity is correct, it does demonstrate that it is feasible to numerically evaluate all the integrals in the identity and it provides numerical support for the validity of the identity.

6 Analytic preconditioner (APEFIE) for closed surface PEC targets

6.1 $3d$ scalar

In the process of numerically validating the $2d$ PBI we came to the realization that, while the $2d$ PBI affords the advantage of achieving an *explicitly* second kind integral operator, it may still be possible to construct a numerical representation of the double Hilbert transform operator in such a way that its desirable spectral properties are not compromised. The advantage of the latter approach is that it is easier and less time consuming to compute the double Hilbert transform than the PBI integral. If we could make do with the double Hilbert transform alone, we could speed up the calculation of the near interaction matrix elements in the analytically preconditioned EFIE considerably.

Analytically, the double Hilbert integral behaves like a second kind operator. Its spectrum consists of several distinct eigenvalues corresponding to low frequency eigenmodes plus a collection of eigenvalues piling up at $\frac{1}{4}$. The eigenvalues at $\frac{1}{4}$ correspond to the higher frequency eigenmodes. The

problem we previously observed was that numerical representations of this operator did not display second kind behavior. The spectrum of the discretized double Hilbert transform consisted of lower frequency eigenvalues that were well resolved and higher frequency ones that were not. Instead of all the eigenvalues corresponding to higher frequency eigenmodes collecting at $\frac{1}{4}$, we observed a trail of eigenvalues extending from $\frac{1}{4}$ to the origin.

The problem had to do with the way we were discretizing the double Hilbert transform term. The double Hilbert transform operator is the composition of two Hilbert transforms. If we define the individual Hilbert transform operators as in (19), then the double Hilbert transform operator in (20a) is

$$H_{12} = H_1 H_2$$

In the past we had been computing the matrix representation of H_{12} ($= I_{DHT}$) as the product of the matrix representations of H_1 and H_2. If S represents a single patch containing N sample points, then the matrix representation of H_2 was a square matrix connecting the N source points $\mathbf{x}''$ to N intermediate field points $\mathbf{x}'$; and H_1 was a square matrix connecting the N intermediate source points $\mathbf{x}'$ to the N field points $\mathbf{x}$. The resultant product matrix H_{12} connects the N source points $\mathbf{x}''$ to the N field points $\mathbf{x}$ as it should.

As part of the process of validating the $2d$ PBI, we computed the matrix representation of H_{12} two new ways. The first way was to compute H_{12} "all at once". In other words, we computed the outer integral term in

$$H_{12}\left(\psi\left(\mathbf{x}\right)\right) = \int_S ds'\ \phi_1\left(\mathbf{x}'\right)\left(\widehat{\mathbf{n}} \times \nabla G\left(\mathbf{x}, \mathbf{x}'\right)\right) \cdot \int_S ds''\ \phi_2\left(\mathbf{x}''\right)\left(\widehat{\mathbf{n}}'' \times \nabla'' G\left(\mathbf{x}', \mathbf{x}''\right)\right) \psi\left(\mathbf{x}''\right) \tag{21}$$

adaptively while also using adaptive integration to evaluate the inner integral at each quadrature point of the outer integration. The second way is much like the method described in the previous paragraph except that we used M intermediate source/field points $\mathbf{x}'$ in the calculation of the individual matrix representations, where $M > N$. The matrix representations of H_1 and H_2 became complementary rectangles rather than squares. The final result for H_{12} is, of course, still square.

We computed the spectrum of H_{12} for a sphere using all three techniques. As before, we found that the original technique produced a trail of

eigenvalues from $\frac{1}{4}$ to the origin, which correspond to unresolved high spatial frequency eigenmodes on the sphere. When we did the same calculation using either of the two new ways this was not the case. Instead, we saw the correct spectrum. For the all-at-once evaluation method this is as expected – the full operator is being computed to whatever accuracy is specified so the spectrum should be similarly accurate. However, we found that it also worked for the matrix product method when M was only modestly larger than N. In particular, we found that doubling the sample point density in each surface dimension (i.e., $M = 4N$) was generally sufficient to recover the correct spectral properties. This method of evaluation is generally much faster than the all-at-once method, which, in turn, is much faster than evaluating the PBI integral. When $M \gg N$, results obtained using the matrix product method should become indistinguishable from those obtained using the all-at-once method given that both methods will be employing a large number of intermediate sample points distributed over the surface in their computations.

The following plot demonstrates the difference between the old and new ways of computing the double Hilbert transform term. The plot shows eigenvalues for the double Hilbert transform operator on an $r = 0.43667\lambda$ sphere. The red points labeled "old way" were computed using the matrix product method with the number of intermediate points equaling the number of field/source points on each patch. The green points were computed using the all-at-once integration method. The blue points are the analytically computed eigenvalues[3] of the double Hilbert transform operator on the sphere. The computation was performed using a low order discretization so the red and green eigenvalues are seen to converge rather slowly to the exact blue ones. The salient feature of the plot is the difference in the behavior of the red and green points corresponding to high spatial frequency modes. The red eigenvalues form a trail extending from $(0.25, 0)$ to the origin. By contrast, the green eigenvalues tend to accumulate near $(0.25, 0)$, as they should.

6.2 $3d$ vector EM

The $3d$ vector EM analogs of the product operator $H_1 H_2$ in (21) are the product operators $T^\alpha T^T$ and $T^\beta T^L$ defined in (14). Together they constitute

[3]The l^{th} eigenvalue for the double Hilbert transform operator on a sphere of radius r is $-l\,(l+1)\left(\frac{\mathbb{J}_l(kr)\mathbb{H}_l(kr)}{kr}\right)^2$, where $\mathbb{J}_l$ and $\mathbb{H}_l$ are the Riccati-Bessel and Riccati-Hankel functions, respectively, of order l.

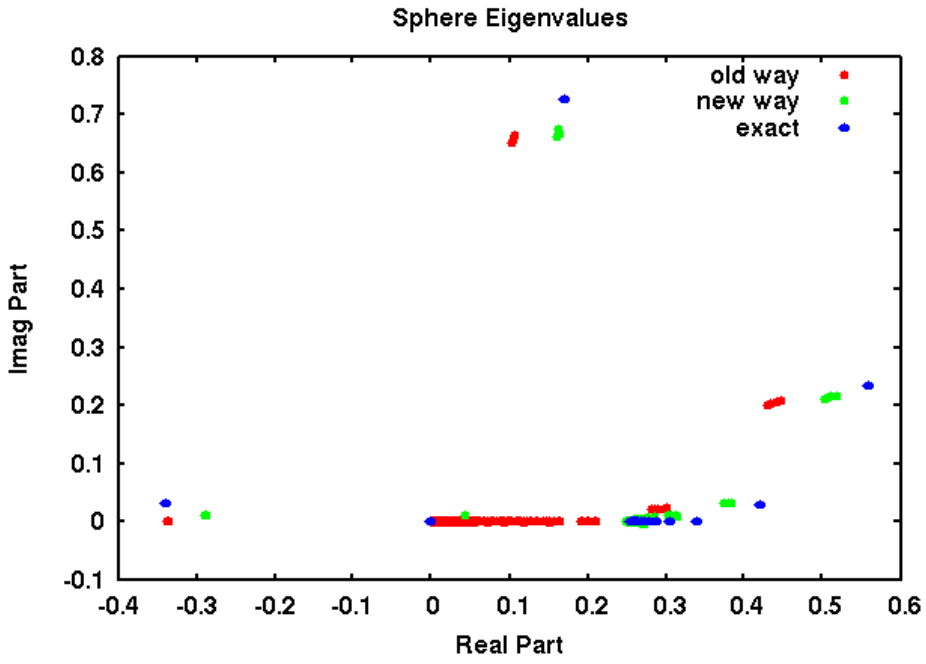

Figure 1: Eigenvalues spectrum for double Hilbert transform operator on a sphere.

the second kind part of the T^2 operator. In our original implementation of the Analytically Preconditioned Electric Field Integral Equation (APEFIE), we obtained a matrix representation for T^2 by separately discretizing its component operators T^α, T^T, T^β, T^L, and T^S, multiplying them in pairs, and adding them together. The matrix representation of each operator was square. The numerical spectrum exhibited eigenvalues tending toward the origin just as we saw in the scalar case because the discretized operator was under-resolving high spatial frequency eigenmodes that the discretization was capable of representing.

In our original implementation we overcame this problem by adding the magnetic field equation (MFIE) to the TTIE[4] to create a combined field equation (CFIE). This not only moves the low-pass filtered eigenvalues of T^2 away from the origin by virtue of the constant term (one half) contributed

[4]TTIE is an alternative abbreviation for APEFIE. The name evokes the fact that it is based on the TT operator.

by the MFIE, it also eliminates spurious resonances. In the present case, we were able to solve the problem by slightly over-resolving the discretization at intermediate points of the product operator like we did for the double Hilbert transform operator in the scalar case. This approach has the advantage that it can also be extended to the open surface case where adding the MFIE is not an option.

Figures 2, 3, and 4 compare the spectrum of the TTIE computed the old way (with the number of intermediate sample points equal to the number of field/source points) and the new way (with the four times a many intermediate sample points as field/source points). In these plots, the red points are for the old discretization method (a standard iterative EFIE solver), the green points are for the new discretization method (more intermediate sample points), and the blue points are the analytical result. Of the three targets one expects the spectral behavior of the APEFIE to be ideal only for the sphere because its surface is smooth. By contrast, the cube has sharp edges and corners and the ogive has pointy tips, all of which are geometric singularities. The *ideal* APEFIE for targets with such geometric singularities probably incorporates complementary singularity functions in the APEFIE operator (see discussion in the next section). Although we did not do that, the computed spectra of the APEFIE operators for the cube and ogive have the characteristics one desires in the ideal operator, namely a bounded spectrum and an eigenvalue collection point well separated from the origin.

7 Analytic preconditioner for open surface PEC targets

The APEFIE overcomes the local causes of EFIE ill conditioning on smooth targets for which the source distribution is also expected to be smooth and continuous. Open surfaces are not smooth targets and one expects the source distribution to exhibit singular behavior near an open edge. Therefore, it should not be surprising if the ideal analytic preconditioner for open surface PEC targets turns out to be different from the APEFIE for closed surface PEC targets. In fact, the quest for the ideal APEFIE for open surfaces may provide some insight into what the ideal APEFIE for closed surface targets with geometric singularities (edges, corners, sharp tips, etc.) should look like.

To get some insight into what the ideal APEFIE for open surface targets should look like, it is helpful to first analyze the problem of scalar scattering

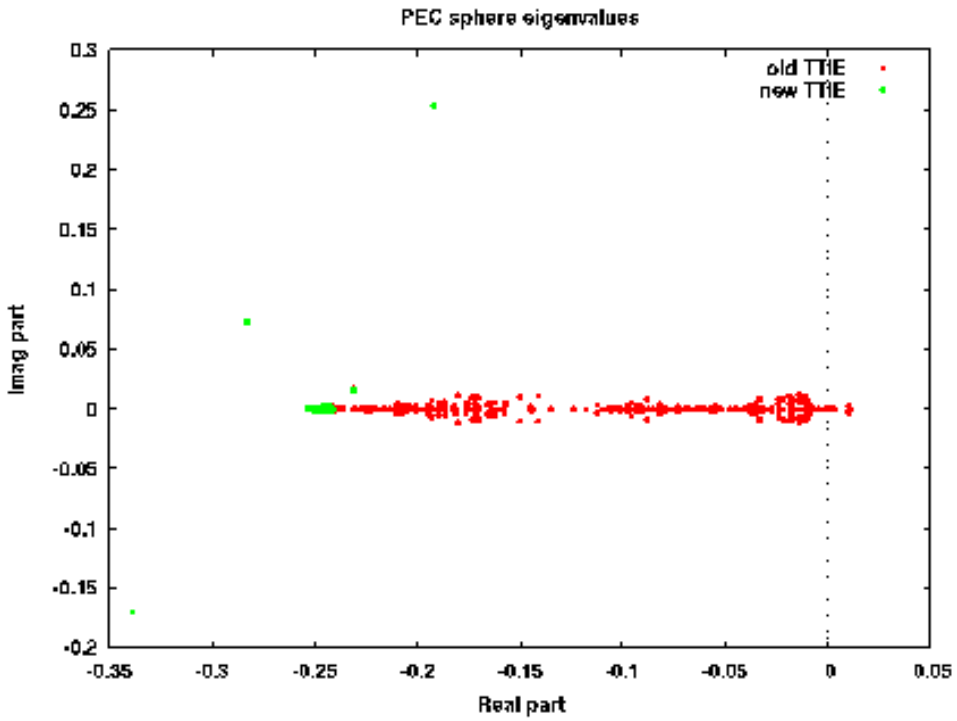

Figure 2: Eigenvalue spectrum for the APEFIE on a PEC sphere with radius $r = \frac{1}{2}\lambda$, comparing old (red) and new (green) discretization methods.

from open surface targets in $2d$ and $3d$. In both cases, analytical solutions are available for scattering from simple canonical targets. The solutions are particularly simple in the Laplace limit, which is sufficient for analyzing the local behavior of the operators. Unfortunately, there is, as yet, no simple analytical solution for the $3d$ EM vector case[5].

7.1 Analytical solutions

7.1.1 $2d$ scalar case

The $2d$ scalar analogs of the EFIE are (4) and (5) and the canonical open surface target for $2d$ scalar scattering is a flat strip.

[5]There are series solutions (e.g., [12]) for scattering from a flat PEC disc but they are quite complicated and do not offer immediate insight into the modes of the EFIE operator on the disc.

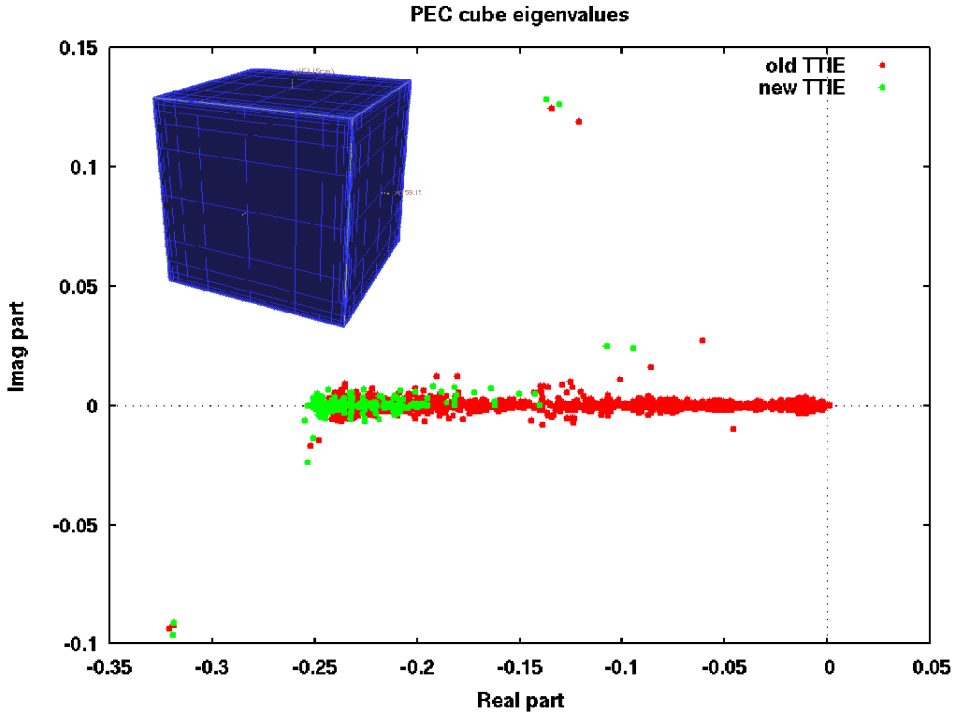

Figure 3: Eigenvalue spectrum for the APEFIE on a cube with 1λ sides, comparing old (red) and new (green) discretization methods.

Dirichlet boundary conditions

First consider (4), which is the appropriate integral equation for $2d$ scalar scattering from the curve C under Dirichlet boundary conditions ($\psi = 0$ on C) or, equivalently, TM-polarized $3d$ vector EM scattering from the infinite cylinder with cross section C. Preconditioning (4) by the hypersingular kernel integral operator from (5) followed by an arbitrary scalar function

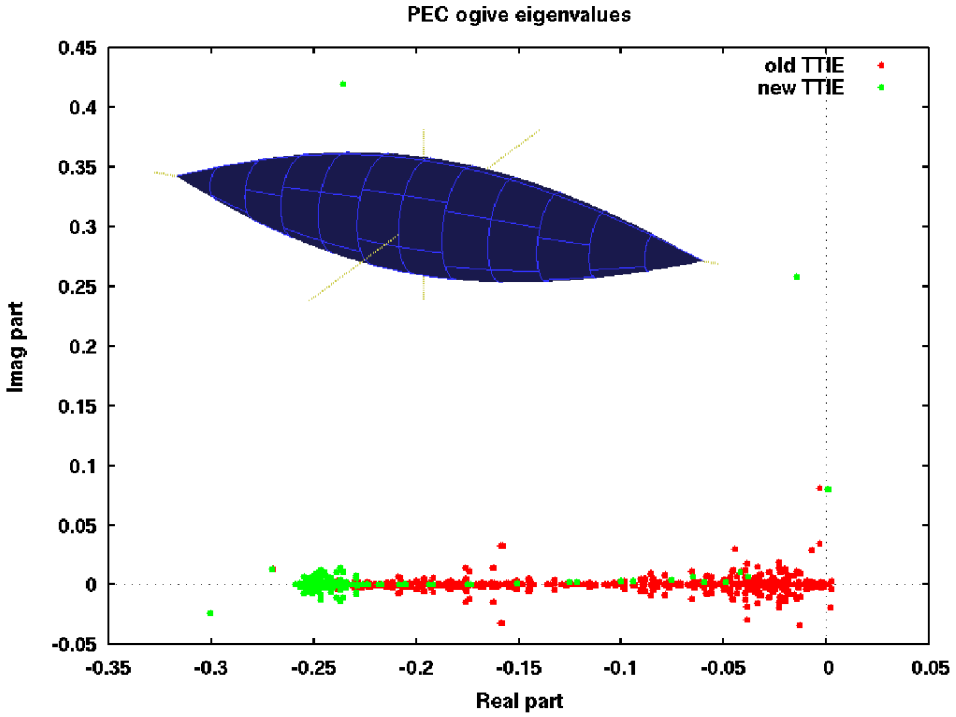

Figure 4: Eigenvalue spectrum for the APEFIE on a PEC ogive with tip-to-tip length $l = 10\lambda$ and center radius $r = 1\lambda$, comparing old (red) and new (green) discretization methods.

$\phi_1(\mathbf{x}')$ gives

$$\begin{aligned}
&\frac{d}{dn}\int_C dl' \frac{\partial G(\mathbf{x},\mathbf{x}')}{\partial n'}\phi_1(\mathbf{x}')\,\psi^{inc}(\mathbf{x}') \\
&= \frac{d}{dn}\int_C dl' \frac{\partial G(\mathbf{x},\mathbf{x}')}{\partial n'}\phi_1(\mathbf{x}')\int_C dl'' G(\mathbf{x}',\mathbf{x}'')\,\frac{d\psi(\mathbf{x}'')}{dn''} \\
&= k^2\int_C dl'\,(\widehat{\mathbf{n}}\cdot\widehat{\mathbf{n}}')\,G(\mathbf{x}',\mathbf{x}'')\,\phi_1(\mathbf{x}')\int_C dl'' G(\mathbf{x}',\mathbf{x}'')\,\frac{d\psi(\mathbf{x}'')}{dn''} \\
&- \frac{d}{dl}\int_C dl' \frac{\partial G(\mathbf{x},\mathbf{x}')}{\partial l'}\phi_1(\mathbf{x}')\int_C dl'' G(\mathbf{x}',\mathbf{x}'')\,\frac{d\psi(\mathbf{x}'')}{dn''}
\end{aligned} \tag{22}$$

where we have also made use of the $2d$ identity [13]

$$\frac{\partial}{\partial n}\frac{\partial G(\mathbf{x},\mathbf{x}')}{\partial n'} = (\widehat{\mathbf{n}}\cdot\widehat{\mathbf{n}}')\,k^2 G(\mathbf{x},\mathbf{x}') - \frac{\partial}{\partial l}\frac{\partial G(\mathbf{x},\mathbf{x}')}{\partial l'}. \tag{23}$$

Using integration by parts we can replace the last term on the far RHS of (22) by

$$
\begin{aligned}
&-\frac{d}{dl}\int_C dl' \frac{\partial G\left(\mathbf{x},\mathbf{x}'\right)}{\partial l'}\phi_1\left(\mathbf{x}'\right)\int_C dl'' G\left(\mathbf{x}',\mathbf{x}''\right)\frac{d\psi\left(\mathbf{x}''\right)}{dn''} \\
&=\int_C dl' \frac{\partial G\left(\mathbf{x},\mathbf{x}'\right)}{\partial l}\phi_1\left(\mathbf{x}'\right)\int_C dl'' \frac{\partial G\left(\mathbf{x}',\mathbf{x}''\right)}{\partial l'}\frac{d\psi\left(\mathbf{x}''\right)}{dn''} \\
&+\int_C dl' \frac{\partial G\left(\mathbf{x},\mathbf{x}'\right)}{\partial l}\frac{d\phi_1\left(\mathbf{x}'\right)}{dl'}\int_C dl'' G\left(\mathbf{x}',\mathbf{x}''\right)\frac{d\psi\left(\mathbf{x}''\right)}{dn''} \\
&-\left[\frac{\partial G\left(\mathbf{x},\mathbf{x}'\right)}{\partial l}\phi_1\left(\mathbf{x}'\right)\int_C dl'' G\left(\mathbf{x}',\mathbf{x}''\right)\frac{d\psi\left(\mathbf{x}''\right)}{dn''}\right]_{\mathbf{x}'=C_1}^{\mathbf{x}'=C_2}
\end{aligned}
\tag{24}
$$

Let us specify C to be the interval from -1 to 1 and let the Green function be the $2d$ Laplace kernel given in (3). For later notational convenience, we will also pull an arbitrary scalar function $\phi_2\left(x''\right)$ out of $\frac{d\psi(\mathbf{x}'')}{dn''}$, i.e., replace $\frac{d\psi(\mathbf{x}'')}{dn''}$ by $\phi_2\left(x''\right)\xi\left(x''\right)$. Then the first term on the far RHS of (24) becomes

$$
\frac{1}{(2\pi)^2}\oint_{-1}^{1} dx' \frac{\phi_1\left(x'\right)}{x-x'}\oint_{-1}^{1} dx'' \frac{\phi_2\left(x''\right)}{x'-x''}\xi\left(x''\right) \tag{25}
$$

which, apart from the constant prefactor, is identical to the LHS of (1).

At this point it is worthwhile to make note of the following standard identities ((22.13.4) and (22.13.3) in [14]):

$$
\oint_{-1}^{1} dx' \frac{1}{x-x'}\sqrt{1-x'^2}U_{n-1}\left(x'\right)=\pi T_n\left(x\right) \tag{26}
$$

$$
\oint_{-1}^{1} dx' \frac{1}{x-x'}\frac{1}{\sqrt{1-x'^2}}T_n\left(x'\right)=-\pi U_{n-1}\left(x\right) \tag{27}
$$

where T_n and U_n represent the n^{th} Chebyshev polynomials of the first and second kind, respectively, and $n=1,2,\ldots$.

If we define

$$
\phi_1\left(x\right)\equiv\sqrt{1-x^2} \text{ and } \phi_2\left(x\right)\equiv 1/\sqrt{1-x^2} \tag{28}
$$

it follows that

$$
\frac{1}{(2\pi)^2}\oint_{-1}^{1} dx' \frac{\phi_1\left(x'\right)}{x-x'}\oint_{-1}^{1} dx'' \frac{\phi_2\left(x''\right)}{x'-x''}T_n\left(x''\right)=-\frac{1}{4}T_n\left(x\right). \tag{29}
$$

for $n = 1, 2, 3, \ldots$. In other words, with this choice for ϕ_1 and ϕ_2, the eigenfunctions of the operator in (25) are the Chebyshev polynomials of the first kind and in all cases the eigenvalue is $-1/4$.

Notes:

- Any smooth function defined on the interval $[-1:1]$ can be expressed as a linear combination of first kind Chebyshev polynomials;
- The product of $\phi_2(x)$ with any linear combination of first kind Chebyshev polynomials will have $1/\sqrt{1 \mp x}$ singularities at the endpoints ± 1 and be regular in the interior of the interval, which matches the endpoint behavior one expects for solutions to (5);
- $\phi_1(x)$ vanishes at the endpoints.
- The identity for $U_n(x)$ corresponding to (29),

$$\frac{1}{(2\pi)^2} \fint_{-1}^{1} dx' \frac{\phi_2(x')}{x - x'} \fint_{-1}^{1} dx'' \frac{\phi_1(x'')}{x' - x''} U_n(x'') = -\frac{1}{4} U_n(x), \qquad (30)$$

  applies for $n = 0, 1, 2 \ldots$. Note the reversed order of the endpoint singularity functions.
- Equations (29) and (30) are special cases of (1) for which the last term on the RHS of (1) evaluates to zero.

Since there is a smooth mapping from the interval $[-1:1]$ to any smooth curve C, we can deduce that the double integral operator

$$\int_C dl' \frac{\partial G(\mathbf{x}, \mathbf{x}')}{\partial l} \phi_1(\mathbf{x}') \int_C dl'' \frac{\partial G(\mathbf{x}', \mathbf{x}'')}{\partial l'} \phi_2(x'') \qquad (31)$$

is a second kind operator. All the other terms in our operator decomposition are compact. Since the difference between the Laplace kernel and the Helmholtz kernel is a regular function, this result also holds for the integral operators associated with $2d$ scattering. Therefore, in the general case, one could write a second kind integration equation for open surface Dirichlet scattering as

$$\begin{aligned} &\frac{d}{dn} \int_C dl' \frac{\partial G(\mathbf{x}, \mathbf{x}')}{\partial n'} \phi_1(\mathbf{x}') \psi^{inc}(\mathbf{x}') \\ &= \frac{d}{dn} \int_C dl' \frac{\partial G(\mathbf{x}, \mathbf{x}')}{\partial n'} \phi_1(\mathbf{x}') \int_C dl'' G(\mathbf{x}', \mathbf{x}'') \phi_2(\mathbf{x}'') \xi(\mathbf{x}''), \end{aligned} \qquad (32)$$

where ϕ_1 and ϕ_2 are complementary endpoint singularity functions like those in (28) and the solution is given by $\frac{d\psi(\mathbf{x}'')}{dn''} = \phi_2(\mathbf{x}'')\,\xi(\mathbf{x}'')$. The eigenvalues for high spatial frequency eigenmodes of the double integral operator on the RHS of (32) will accumulate at $-1/4$.

Note:

- If the curve C was the unit circle (a closed surface) instead of the unit interval (an open surface), a similar analysis results in the same conclusion for Eq. (32). The only difference is that the functions ϕ_1 and ϕ_2 both equal one. The same analysis is extensible to the case where C is any smooth closed curve.

Neumann boundary conditions

A similar result obtains for $2d$ scalar scattering from the curve C under Neumann boundary conditions ($\partial_n\psi = 0$ on C) or, equivalently, TE-polarized $3d$ vector EM scattering from the infinite cylinder with cross section C. In this case, however, it is more convenient to make use of a postconditioning operator that contains the complementary kernel singularity and the complementary singularity factor[6].

It works like this. Assume that we can write ψ as

$$\psi(\mathbf{x}') = \phi_1(\mathbf{x}') \int_C dl'' G(\mathbf{x}', \mathbf{x}'')\,\phi_2(\mathbf{x}'')\,\xi(\mathbf{x}'') \tag{33}$$

for some functions $\phi_1(\mathbf{x}')$ and $\xi(\mathbf{x}'')$, in which case we can rewrite (5) as

$$-\frac{d\psi^{inc}(\mathbf{x})}{dn} = \frac{d}{dn}\int_C dl' \frac{\partial G(\mathbf{x}, \mathbf{x}')}{\partial n'}\phi_1(\mathbf{x}') \int_C dl'' G(\mathbf{x}', \mathbf{x}'')\,\phi_2(\mathbf{x}'')\,\xi(\mathbf{x}'')\,. \tag{34}$$

After applying (23) and using integration by parts as before, we can

[6]Preconditioning by the same operator would also result in a second kind operator for ψ. However, one cannot manipulate it into a sum of compact operators and a double Hilbert transform operator because the integration by parts procedure produces a term whose integrand is proportional to $\frac{d\phi_2(\mathbf{x}')}{dx'} \sim (1 - x'^2)^{-3/2}$, which is not an integrable endpoint singularity.

rewrite the RHS of (34) as

$$\begin{aligned}
&\int_C dl' \frac{\partial G\left(\mathbf{x},\mathbf{x}'\right)}{\partial l}\phi_1\left(\mathbf{x}'\right)\int_C dl'' \frac{\partial G\left(\mathbf{x}',\mathbf{x}''\right)}{\partial l'}\phi_2\left(\mathbf{x}''\right)\xi\left(\mathbf{x}''\right)\\
&+\int_C dl' \frac{\partial G\left(\mathbf{x},\mathbf{x}'\right)}{\partial l}\frac{\partial \phi_1\left(\mathbf{x}'\right)}{\partial l'}\int_C dl'' G\left(\mathbf{x}',\mathbf{x}''\right)\phi_2\left(\mathbf{x}''\right)\xi\left(\mathbf{x}''\right)\\
&-k^2\int_C dl'\left(\widehat{\mathbf{n}}\cdot\widehat{\mathbf{n}}'\right)G\left(\mathbf{x},\mathbf{x}'\right)\phi_1\left(\mathbf{x}'\right)\int_C dl'' G\left(\mathbf{x}',\mathbf{x}''\right)\phi_2\left(\mathbf{x}''\right)\xi\left(\mathbf{x}''\right)\\
&-\left[\frac{\partial G\left(\mathbf{x},\mathbf{x}'\right)}{\partial l}\phi_1\left(\mathbf{x}'\right)\int_C dl'' G\left(\mathbf{x}',\mathbf{x}''\right)\phi_2\left(\mathbf{x}''\right)\xi\left(\mathbf{x}''\right)\right]_{\mathbf{x}'=C_1}^{\mathbf{x}'=C_2} \qquad (35)
\end{aligned}$$

Following the same arguments as in the Dirichlet case we find that the first term in (35) is second kind with respect to ξ whereas the other terms are compact operators or zero. Therefore (34) is a second kind integral equation for open surface Neumann scattering. Having obtained a solution for ξ, the solution for ψ follows immediately from (33).

7.1.2 $3d$ scalar case

The equations describing scalar wave scattering under Dirichlet and Neumann boundary conditions in $3d$ are the same as (4) and (5) except that the integrals over curve C must be replaced by integrals over surface S. The canonical open surface target for $3d$ scattering is a flat circular disc.

The analytical preconditioning procedure is similar to what we did in the $2d$ scalar case, i.e., pre- or postcondition each integral equation by an integral operator that includes the complementary kernel singularity and the edge singularity factor that is complementary to the expected source term edge singularity. The rest of the procedure follows much the same path as before. The important differences are in the details of the second kind term, which we can analyze in the Laplace limit for the specific case where S is the unit disc.

Oblate spheroidal coordinates are ideal for analyzing the disc problem because the $3d$ scalar Helmholtz and Laplace equations are separable in this coordinate system $\{\xi,\eta,\varphi\}$ and the degenerate ($\xi\to 0$) limit of an oblate spheroid is a flat disc. Two views of the oblate coordinate system on a disc are shown in Fig. 5. The two oblate spheroidal coordinates that describe a disc are φ and η. The φ coordinate is the usual azimuthal coordinate. On a disc of radius a, the η coordinate is related to the radius by $r = a\left(1-\eta^2\right)^{1/2}$.

Note:

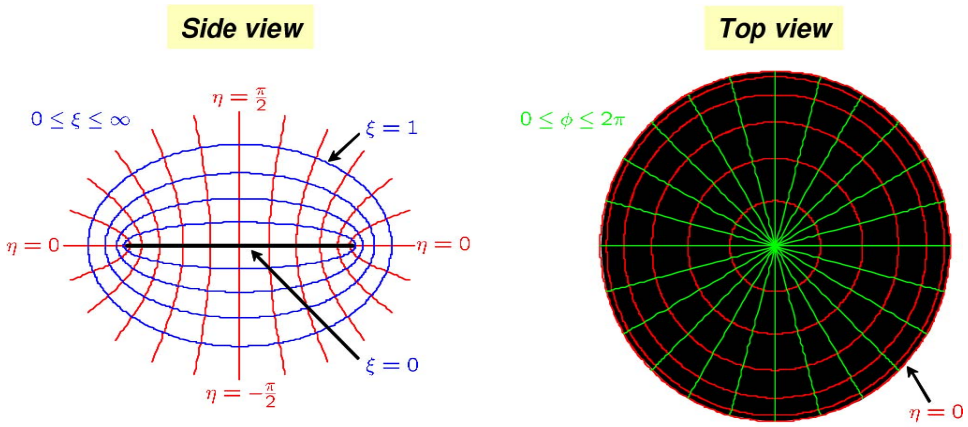

Figure 5: Oblate spheroidal coordinate system

- Since $\eta = \left(1 - (r/a)^2\right)^{1/2}$, one expects solutions to the Dirichlet problem to scale like $1/\eta$ near the edge of the disc and solutions to the Neumann problem to scale like η near the edge of the disc. In other words, η and $1/\eta$ can serve as complementary edge singularity functions.
- As η runs from -1 to 0 to $+1$, the location on the disc runs from the underside center, to the edge, to the topside center.

Solutions to the Laplace equation on the disc are linear combinations of modes of the form

$$\psi_{lm}(\eta, \varphi) \equiv P_l^m(\eta)\, e^{im\varphi} \tag{36}$$

where $P_l^m(\eta)$ is the associated Legendre function of order (l, m). The function $P_l^m(\eta)$ is an even (odd) polynomial in η times r^m for $l+m$ even (odd).

Solutions to the Helmholtz equation with wavenumber k on the disc are linear combinations of modes of the form

$$\psi_{lm}(\eta, \varphi; \gamma) \equiv S_l^m(\eta, \gamma)\, e^{im\varphi} \tag{37}$$

where $S_l^m(\eta, \gamma)$ is the oblate spheroidal wavefunctions of order (l, m) and dimensionless scale size $\gamma = ka$. Unlike the associated Legendre functions, the oblate spheroidal wavefunctions do not have a simple closed form. Nor do they obey most of the simple identities that the associated Legendre

polynomials obey (see 8.73-8.74 of [15]). In the low frequency limit, they reduce to associated Legendre functions, i.e.,

$$S_l^m(\eta,\gamma) \to P_l^m(\eta) \text{ as } \gamma \to 0.$$

The key ingredients for the analysis are:

- Angular orthogonality:

$$\int_0^{2\pi} d\varphi \; e^{i(m-m')\varphi} = 2\pi\delta_{m,m'}$$

- Radial orthogonality ((7.112.1) of [15]):

$$\int_{-1}^{1} d\eta \; P_l^{|m|}(\eta) \, P_{l'}^{|m|}(\eta) = \frac{2}{2l+1}\frac{(l+|m|)!}{(l-|m|)!}\delta_{l,l'}$$

- Differential area element:

$$dA = a^2 \, |\eta| \, d\eta \, d\varphi$$

(Note that $a^2 \int_0^{2\pi} d\varphi \int_{-1}^{1} |\eta| \, d\eta$ covers the disc twice – once over the top side and once over the bottom side.)

- Laplace Green function expansion (derived from (10.3.63) of [16]) in terms of Laplace modes $\left(P_l^{|m|}(\eta)\, e^{im\varphi}\right)$:

$$G(\mathbf{x},\mathbf{x}') = \frac{1}{4\pi a}\sum_{l=0}^{\infty}\sum_{\substack{m=-l \\ \text{(by 2)}}}^{l} \frac{2l+1}{c_{lm}}\frac{(l-|m|)!}{(l+|m|)!} P_l^{|m|}(\eta) \, P_l^{|m|}(\eta') \, e^{im(\varphi-\varphi')} \tag{38}$$

where a is the radius of the disc and

$$c_{lm} \equiv 2\frac{\Gamma\left(\frac{l+m+2}{2}\right)\Gamma\left(\frac{l-m+2}{2}\right)}{\Gamma\left(\frac{l+m+1}{2}\right)\Gamma\left(\frac{l-m+1}{2}\right)}. \tag{39}$$

With these relations we obtained the following analytical results[7] when S is disc of radius a and G is the Laplace kernel:

- First kind and hypersingular integral operators including edge singularity factors:

$$\int_S ds'\, G\left(\mathbf{x},\mathbf{x}'\right)\frac{1}{\eta'}\psi_{lm}\left(\eta',\varphi'\right)=\frac{a}{2c_{lm}}\psi_{lm}\left(\eta,\varphi\right)\quad \text{for } l+m \text{ even} \tag{40}$$

and

$$\frac{d}{dn}\int_S ds'\frac{\partial G\left(\mathbf{x},\mathbf{x}'\right)}{\partial n'}\eta'\left(\frac{\psi_{lm}\left(\eta',\varphi'\right)}{\eta'}\right)=\frac{c_{lm}}{2a}\frac{\psi_{lm}\left(\eta,\varphi\right)}{\eta}\quad \text{for } l+m \text{ odd} \tag{41}$$

where $\psi_{lm}\left(\eta,\varphi\right)$ is the scalar Laplace mode as defined in (36). Note that $\psi_{lm}\left(\eta,\varphi\right)$ is an even (odd) function of η if $l+m$ is even (odd), so $\psi_{lm}\left(\eta,\varphi\right)$ in (40) with $l+m$ is even, and $\frac{\psi_{lm}(\eta,\varphi)}{\eta}$ in (41) with $l+m$ is odd, are both regular functions on the whole of the disc (i.e., for $-1\leq\eta\leq 1$ and $0\leq\varphi\leq 2\pi$) and even functions of η.

- Combinations of first kind and hypersingular integral operators including edge singularity factors:

$$\begin{aligned}&-\frac{d}{dn}\int_S ds'\frac{\partial G\left(\mathbf{x},\mathbf{x}'\right)}{\partial n'}\eta'\int_S ds''\, G\left(\mathbf{x}',\mathbf{x}''\right)\frac{1}{\eta''}\psi_{lm}\left(\eta'',\varphi''\right)\\&=\sum_{\substack{l'=m\\(\text{by } 2)}}^{l}\alpha_{lm}^{l'}\psi_{l'm}\left(\eta,\varphi\right)\quad \text{for } l+m \text{ even}\end{aligned} \tag{42}$$

and

$$\begin{aligned}&-\int_S ds'\, G\left(\mathbf{x},\mathbf{x}'\right)\frac{1}{\eta'}\frac{d}{dn'}\int_S ds''\frac{\partial G\left(\mathbf{x}',\mathbf{x}''\right)}{\partial n''}\eta''\left(\frac{\psi_{lm}\left(\eta'',\varphi''\right)}{\eta''}\right)\\&=\sum_{\substack{l'=m+1\\(\text{by } 2)}}^{l}\beta_{lm}^{l'}\frac{\psi_{l'm}\left(\eta,\varphi\right)}{\eta}\quad \text{for } l+m \text{ odd}\end{aligned} \tag{43}$$

where $\alpha_{lm}^{l'}$ and $\beta_{lm}^{l'}$ are (unspecified) constant coefficients.

[7] As far as we know, these identities are novel results.

- The integral operator in (42) does not mix m's. For a given (l,m) with $l+m$ even, the eigenfunctions of this operator are linear combinations of $\psi_{l'm}(\eta,\varphi)$ with $l'=l,l-2,,\ldots m$. The eigenvalue corresponding to the $(l,m)^{th}$ eigenfunction is

$$-\frac{1}{4}\frac{(l+1)^2-m^2}{c_{lm}^2}. \tag{44}$$

Likewise, the integral operator in (43) does not mix m's. For a given (l,m) with $l+m$ odd, the eigenfunctions of this operator are linear combinations of $\frac{\psi_{l'm}(\eta,\varphi)}{\eta}$ with $l'=l,l-2,,\ldots m+1$. The eigenvalue corresponding to the $(l,m)^{th}$ eigenfunction is

$$-\frac{1}{4}\frac{c_{lm}^2}{l^2-m^2}. \tag{45}$$

- Combinations of Hilbert-transform-like integral operators including edge singularity factors:

$$\begin{aligned}&\int_S ds'\ \widehat{\mathbf{n}}\times\nabla G\left(\mathbf{x},\mathbf{x}'\right)\cdot\eta'\int_S ds''\ \widehat{\mathbf{n}}'\times\nabla' G\left(\mathbf{x}',\mathbf{x}''\right)\frac{1}{\eta''}\psi_{lm}\left(\eta'',\varphi''\right)\\&=-\frac{1}{4}\frac{l\left(l+1\right)-m^2}{c_{lm}^2}\psi_{lm}\left(\eta,\varphi\right)\quad\text{for } l+m \text{ even}\end{aligned} \tag{46}$$

and

$$\begin{aligned}&\int_S ds'\ \widehat{\mathbf{n}}\times\nabla G\left(\mathbf{x},\mathbf{x}'\right)\cdot\frac{1}{\eta'}\int_S ds''\ \widehat{\mathbf{n}}'\times\nabla' G\left(\mathbf{x}',\mathbf{x}''\right)\eta''\left(\frac{\psi_{lm}\left(\eta'',\varphi''\right)}{\eta''}\right)\\&=-\frac{1}{4}\frac{\left(l\left(l+1\right)-m^2\right)c_{lm}^2}{\left(\left(l+1\right)^2-m^2\right)\left(l^2-m^2\right)}\frac{\psi_{lm}\left(\eta,\varphi\right)}{\eta}\quad\text{for } l+m \text{ odd},\end{aligned} \tag{47}$$

Dirichlet boundary conditions

The integral equation appropriate to Dirichlet boundary conditions is (4) with curve C replaced by surface S. Preconditioning both sides of this equation by the surface form of the hypersingular integral operator from (5) followed by an arbitrary surface function $\phi_1(\mathbf{x}')$ gives the surface analog to (22), namely

$$\begin{aligned}&-\frac{d}{dn}\int_S ds'\frac{\partial G\left(\mathbf{x},\mathbf{x}'\right)}{\partial n'}\phi_1\left(\mathbf{x}'\right)\psi^{inc}\left(\mathbf{x}'\right)\\&=-\frac{d}{dn}\int_S ds'\frac{\partial G\left(\mathbf{x},\mathbf{x}'\right)}{\partial n'}\phi_1\left(\mathbf{x}'\right)\int_S ds'' G\left(\mathbf{x}',\mathbf{x}''\right)\phi_2\left(\mathbf{x}''\right)\xi\left(\mathbf{x}''\right),\end{aligned} \tag{48}$$

where we have substituted $\phi_2(\mathbf{x}'')\,\xi(\mathbf{x}'')$ for $\frac{d\psi(\mathbf{x}'')}{dn''}$. Letting $\phi_1(\mathbf{x}') = \eta'$ and $\phi_2(\mathbf{x}'') = 1/\eta''$ puts the RHS of (48) into the same form as the integral operator in (42). The eigenfunctions of this operator are regular functions of position on the disc. The added factor of $\phi_2(\mathbf{x}'') = 1/\eta''$ gives them the correct edge singularity behavior for scalar solutions to the Laplace or Helmholtz problem on the disc under Dirichlet boundary conditions. The eigenvalues of the integral operator in (48) in the Laplace limit can be deduced from (44).

Alternatively, one can take (48) a step further, using the identity [13]

$$\frac{\partial}{\partial n}\frac{\partial G(\mathbf{x},\mathbf{x}')}{\partial n'} = \left(\widehat{\mathbf{n}}\cdot\widehat{\mathbf{n}}'\right)k^2 G\left(\mathbf{x},\mathbf{x}'\right) - \left(\widehat{\mathbf{n}}\times\nabla\right)\cdot\left(\widehat{\mathbf{n}}'\times\nabla'\right)G\left(\mathbf{x},\mathbf{x}'\right) \quad (49)$$

and performing an integration by parts as was done in the $2d$ scalar case. The resulting RHS is the sum of a compact operator and the term[8]

$$\int_S ds' \ \left(\widehat{\mathbf{n}}\times\nabla G\left(\mathbf{x},\mathbf{x}'\right)\right)\cdot\phi_1\left(\mathbf{x}'\right)\int_S ds'' \ \left(\widehat{\mathbf{n}}'\times\nabla' G\left(\mathbf{x}',\mathbf{x}''\right)\right)\phi_2\left(\mathbf{x}''\right)\xi\left(\mathbf{x}''\right) \quad (50)$$

where $\phi_1(\mathbf{x}')$, $\phi_2(\mathbf{x}'')$, and $\xi(\mathbf{x}'')$ are defined as before. The eigenfunctions and corresponding eigenvalues of this operator in the Laplace limit are given by (46).

Neumann boundary conditions

A similar result obtains for Neumann boundary conditions. There are two ways to go about it. One can either precondition the integral equation appropriate to Neumann boundary conditions by the integral operator from the Dirichlet problem or use the post-conditioner approach described previously for $2d$ scalar scattering under Neumann boundary conditions.

In the first case, the integral operator consists of a compact term and a term of the form

$$-\int_S ds' \ G\left(\mathbf{x},\mathbf{x}'\right)\phi_2\left(\mathbf{x}'\right)\frac{d}{dn'}\int_S ds''\frac{\partial G(\mathbf{x}',\mathbf{x}'')}{\partial n''}\phi_1\left(\mathbf{x}''\right)\xi\left(\mathbf{x}''\right) \quad (51)$$

where $\psi(\mathbf{x}'')$ has been replaced by $\phi_1(\mathbf{x}'')\,\xi(\mathbf{x}'')$. Letting $\phi_1(\mathbf{x}'') = \eta''$ and $\phi_2(\mathbf{x}') = 1/\eta'$ puts (51) into the same form as the operator in (42), whose eigenvalues (in the Laplace limit) are given by (45). In the second case, the

[8] This operator in differs from the double Hilbert transform operator $-H_{12}$ defined in (21) by at most a compact operator.

integral operator consists of a compact term and a term identical to that of (50), where $\phi_1(\mathbf{x}')$ and $\phi_2(\mathbf{x}'')$ are defined as above. In both cases, the added factor of $\phi_1(\mathbf{x}'') = \eta''$ in the expression for the solution guarantees that it exhibits the correct edge singularity behavior for the solutions under Neumann boundary conditions.

Second kind character of the eigenvalue spectrum

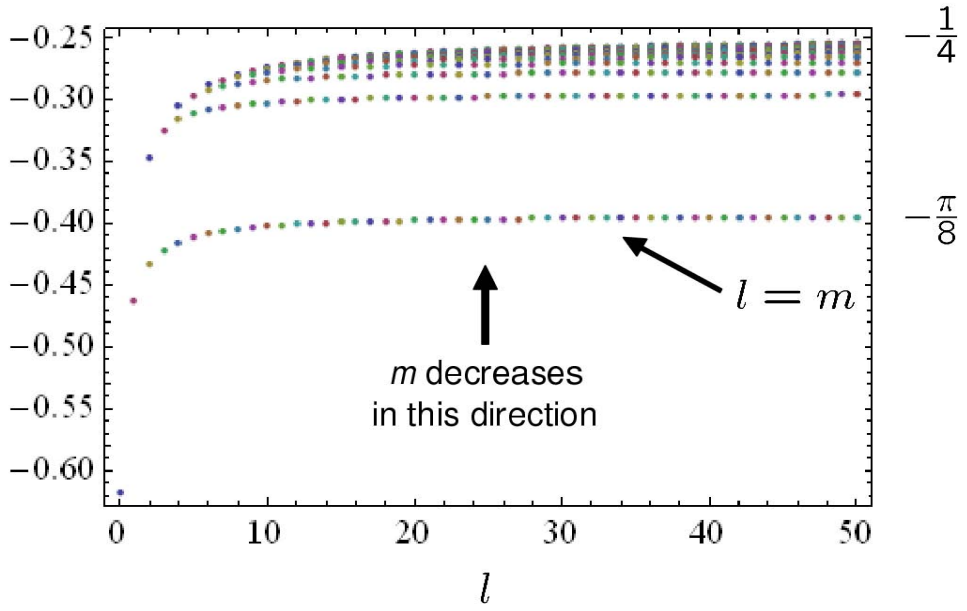

Figure 6: Spectrum of the $3d$ scalar double integral operator in (42) in the Laplace limit; i.e., a plot of the eigenvalues given in (44).

The eigenvalue spectrum in the $3d$ scalar case is not as simple as it was in the $2d$ scalar case wherein the eigenvalue associated with every eigenfunction was $-\frac{1}{4}$. In the $3d$ scalar case, it depends on l and m. For example, Figure 6 is a plot of the Dirichlet eigenvalues[9] in the Laplace limit for $0 \leq m \leq l$

[9]By virtue of the identity $\frac{(l+1)^2-m^2}{c^2_{lm}} = \frac{c^2_{l+1,m}}{(l+1)^2-m^2}$, the eigenvalue spectrum for the Neumann case as a function of $l+1$ is the same as the Dirichlet spectrum as a function of $l.$, i.e. the Neumann counterpart to Figure 6 would look the same except that all points would be shifted rightward by one unit. The spectrum of (50) is the same as the Dirchlet spectrum shown in Figure 6.

up to $l = 50$. In the high spatial frequency limit ($l \to \infty$), the eigenvalues asymptotically approach collection points whose values depend on $l - m$. The number of collection points is infinite, but they all fall into the range from $-\frac{\pi}{8} \simeq -0.393$ to $-\frac{1}{4}$. Obviously, this does not conform to the classic definition of a second kind spectrum because the eigenvalues do not tend to accumulate at a single point. It is more like a sum of second kind operators all of whose eigenvalue collection points are between $-\frac{\pi}{8}$ and $-\frac{1}{4}$. The important point for our purposes is that the spectrum is bounded and all the eigenvalues stay well away from the origin in the high spatial frequency limit.

The corresponding spectrum for the Helmholtz case will be different from that shown above, especially for $l \lesssim ka$. However, the high spatial frequency ($l \to \infty$) behavior of the modes in the Helmholtz case is the same as that in the Laplace case so the above conclusions regarding the limiting behavior of the eigenvalues and the second kind nature of the operator apply equally well to $3d$ scalar scattering.

7.1.3 $3d$ vector EM case

Preconditioning the $3d$ EM vector case is more complicated than either of the previous scalar cases because the EFIE operator has both Dirichlet and Neumann characteristics. The T^S component of T behaves like the Dirichlet operator in (4) and the T^H component of T behaves like the Neumann operator in (5). The vector source distribution also contains both Dirichlet and Neumann characteristics. Near an open edge, the component of the current parallel to the edge obeys $\mathbf{J}_{\parallel} \propto \delta^{-1/2}$ like the Neumann source distribution and the component of the current perpendicular to the edge obeys $\mathbf{J}_{\perp} \propto \delta^{1/2}$ like the Dirichlet source distribution, where δ is the distance to the edge.

We know how to analytically precondition the integral equations for $3d$ scalar scattering under Neumann or Dirichlet boundary conditions, so we might expect some combination of these approaches should work in the $3d$ EM vector case. However, it is not obvious how to do this given the way the EFIE ties them together. Even so, we can make some educated guesses.

Informed by the $1d$ and $2d$ PBI and the ideal analytic preconditioners for $2d$ and $3d$ scalar open surface scattering, we expect that the ideal analytic preconditioner for $3d$ vector EM open surface scattering should look something like this

$$\text{“}T^2\text{”}\mathbf{J} = \left(T^S + T^H\right)\phi_1\left(T^S + T^H\right)\phi_2\mathbf{J} \tag{52}$$

where ϕ_1 and ϕ_2 are complementary edge singularity functions [and $\phi_2\mathbf{J}$ is the source distribution including edge singularity behavior].

We evaluated two versions of "T^2"$\mathbf{J}$ for open surfaces – one in which $\phi_1 = 1$ and another in which ϕ_1 contained the complementary edge singularity to ϕ_2. In both cases, we enforced the correct edge singularity behavior on the currents by incorporating it into the discretization. For a Nyström discretization such as ours, this is done by locating sample points according to a quadrature rule that is high order for integrating the appropriate set of singular functions. For example, on quadrilateral patches with one open edge, we can create a suitable $2d$ quadrature rule from the tensor product of $1d$ quadrature rules, one of which is a regular rule (e.g., Gauss-Legendre) and the other is a rule for integrating polynomials times a weighting function with a $\delta^{-1/2}$ singularity at one end of the interval (e.g., Gauss-Jacobi). One can generate other tensor product rules for cases where more than one edge touches an open surface[10]. We have used these rules for the past several years in our general purpose RCS code (FastScat$^{\text{TM}}$) to achieve high order convergence on open surface scattering problems with the EFIE.

We evaluated the properties of the APEFIE operator in (52) on several simple open surfaces, two of which are discussed below. In our numerical experiments the two versions of "T^2"$\mathbf{J}$ behaved similarly.

Triangle-circle target

The triangle-circle (or EMCC wedge-cylinder-plate) target is composed of an equilateral triangle attached to a semicircle. Our seven quadrilateral, handmade mesh[11] is shown in Fig. 7. The discretization of each outer quadrilateral patches is based on a product rule with one singular edge; the discretization for the center quadrilateral is based on a tensor product of regular quadratures. The total (one-sided) surface area is $3.31\lambda^2$.

Figs. 8 and 9 show the eigenvalue spectra for the open surface specific APEFIE given in (52) and the standard EFIE in (8), for independent discretization densities ranging from 20.6 unknowns/λ to 26.7 unknowns/λ. A

[10]When two adjacent edges of a quadrilateral touch open edges the actual geometry includes a corner. We do not know of a high order expansion for the currents at a corner and our product rule quadratures are unlikely to be ideal. However, our experience shows that a tensor product of $\delta^{\pm 1/2}$ quadratures performs much better than low order quadrature rules.

[11]This mesh exemplifies one of the differences between our Nyström discretization and a typical Galerkin discretization. Being patch based rather than edge based, a Nyström discretization allows for a vertex in the middle of an edge.

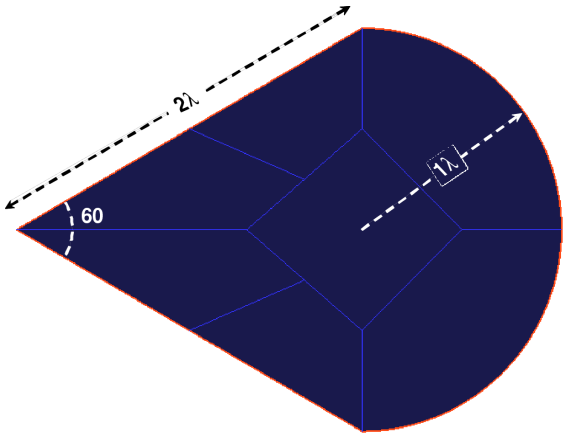

Figure 7: Triangle-circle mesh.

blue dot on top of a green dot on top of a red dot indicates an eigenvalue of a fully resolved eigenmode.

Several features are noteworthy. The eigenvalues of the APEFIE are confined to a relatively small region on the negative real half of the complex plane and tend to cluster about a few points. With few exceptions[12], the eigenvalues have converged. The smallest eigenvalues are still well separated from the origin. By contrast, the EFIE spectrum is spread over a wider region centered about the origin on both halves of the complex plane and is expanding with discretization refinement. The APEFIE spectrum is consistent with a well conditioned operator, the EFIE spectrum is not.

This interpretation is borne out by the iterative solver convergence results shown in Figs. 10 and 11 and summarized in Table 11. The first plot shows residual error vs. iteration count for the transpose-free quasi-minimum residual (TFQMR) iterative solver. The second plot shows the same information for the multiple-RHS generalized minimum residual (MGCR) solver. Note that axes scaling is log - log. In all cases we attempted to solve for the RCS in both polarizations over the azimuthal range from 0° to 180° in 1° steps at 10° elevation. A block diagonal preconditioner based on a block size of $\sim\frac{1}{2}\lambda$ was used with the EFIE to accelerate iterative solver convergence.

[12]The curved tail of unresolved eigenvalues may be connected with the fact that, although our discretization is high order for integrating currents in the interior of the patch and near smooth portions of the edge, it is not high order near corners.

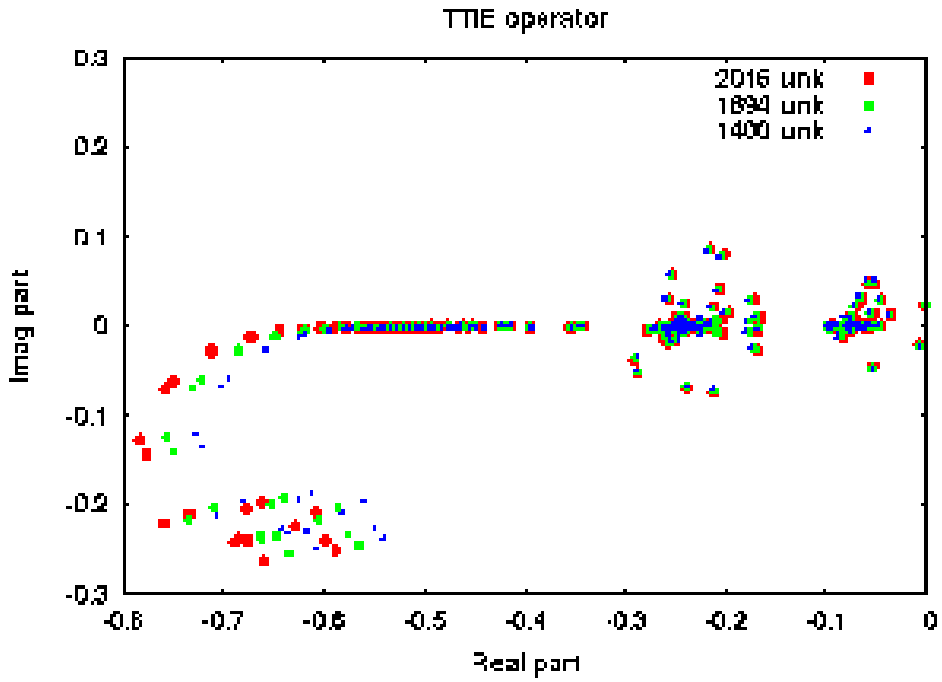

Figure 8: Open surface APEFIE spectrum for triangle-circle target.

The differences in iterative solver convergence for the analytically preconditioned EFIE and the block diagonally preconditioned EFIE are dramatic. The APEFIE consistently converged to a residual error of 10^{-5} in about 30 iterations with the TFQMR and CGS solvers. The EFIE obtained a solution for the first set of excitations in about 50K iterations and was unable to reach the termination condition on the second pass.

The EFIE fared somewhat better with the MGCR solver and the APEFIE fared somewhat worse, but the APEFIE was still almost a factor of 10 faster to converge.

	TTIE	EFIE
TFQMR	∼30	∼60000
CGS	∼30	∼50000
MGCR	∼200	∼1500

Table 11: Number of iterations to convergence.

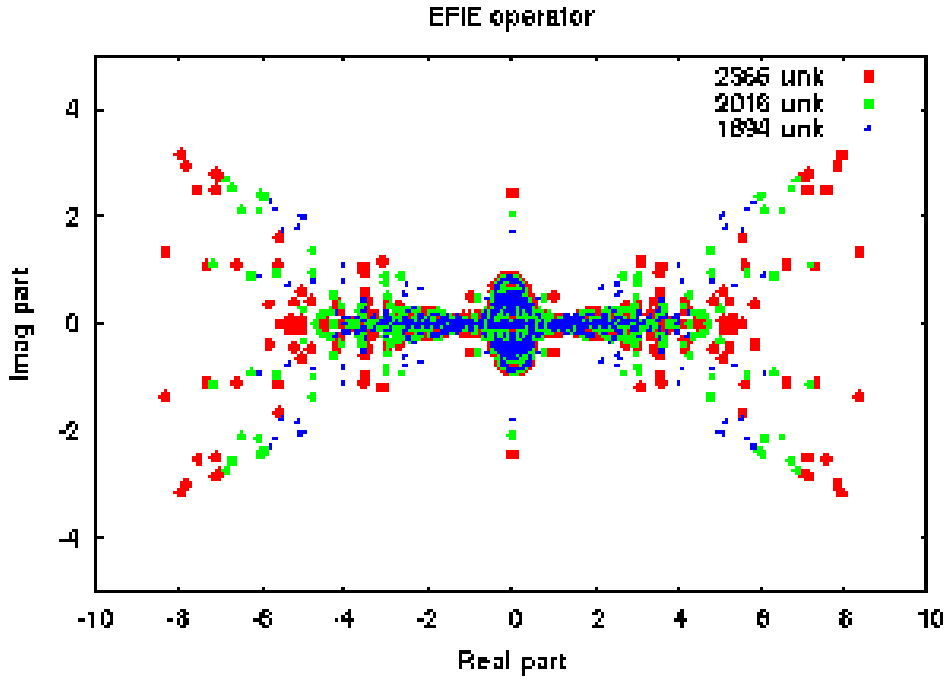

Figure 9: Standard EFIE spectrum for triangle circle target.

RCS results from the APEFIE and EFIE for an H-polarized incident field are compared to the EMCC measurement results in Figs. 12 and 13. Both methods are converging to the same results, although the APEFIE results are slightly more accurate for any given discretization density. All RCS results should be symmetric about 0° since the target is symmetric about 0°. The EMCC measurement data is not symmetric, however, indicating some form of measurement error. We have plotted the two halves of the measurement data on the same $0° - 180°$ scale to provide a crude indication of measurement accuracy.

Our implementation of the Nyström method does not enforce current continuity between patches. Instead, current continuity is a natural consequence of achieving high order convergence to a exact solution that is continuous on a smooth surface. This is generally easier to achieve with a second kind integral operator such as the MFIE and than with an integro-differential operator such as the EFIE.

Current amplitudes on the circle-triangle target computed using the

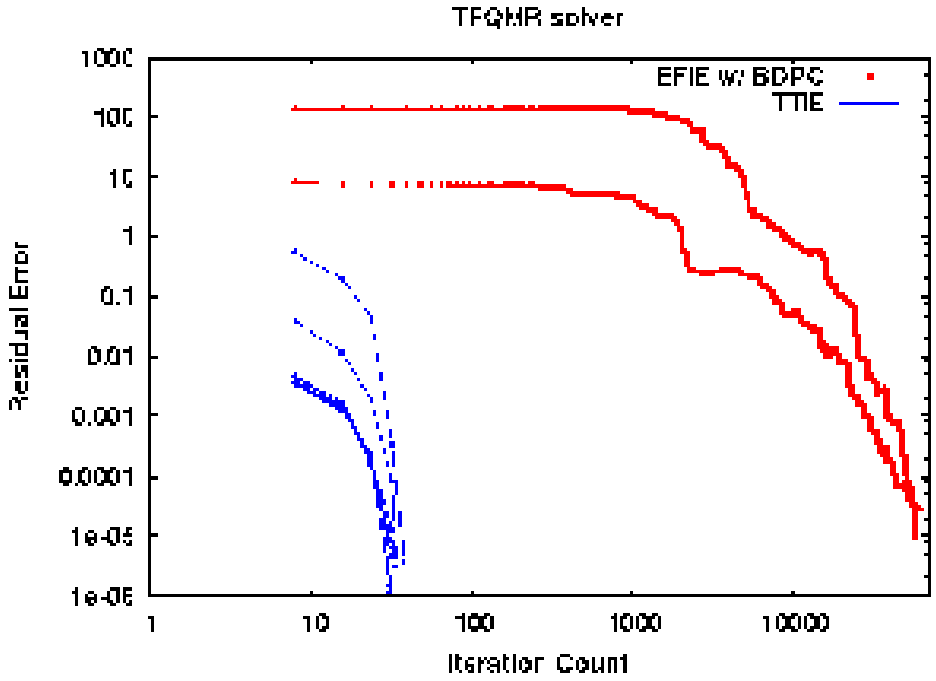

Figure 10: Iterative solver convergence on triangle-circle target using TFQMR solver and EFIE (with a block diagonal preconditioner) and the open surface APEFIE.

APEFIE and EFIE are shown in Figs. 14 and 15. The discretization is the same in both cases: 1694 unknowns (basis order 11). Both current displays exhibit the expected wave pattern and current singularities near edges. The main difference is that the boundaries between patches that are easily visible in the EFIE case are virtually invisible when the APEFIE is used.

A Nyström discretization computes the current only at selected sample points and we determine the currents elsewhere by fitting the sample point data to a high order interpolation function based on the underlying quadrature rule for each patch. Currents at a boundary between patches may be extrapolated from either side. The superior continuity of the APEFIE-computed currents at artificial boundaries is a consequence their Nyström-sampled currents being more accurate, which, in turn, is a consequence of the APEFIE behaving like a second kind operator.

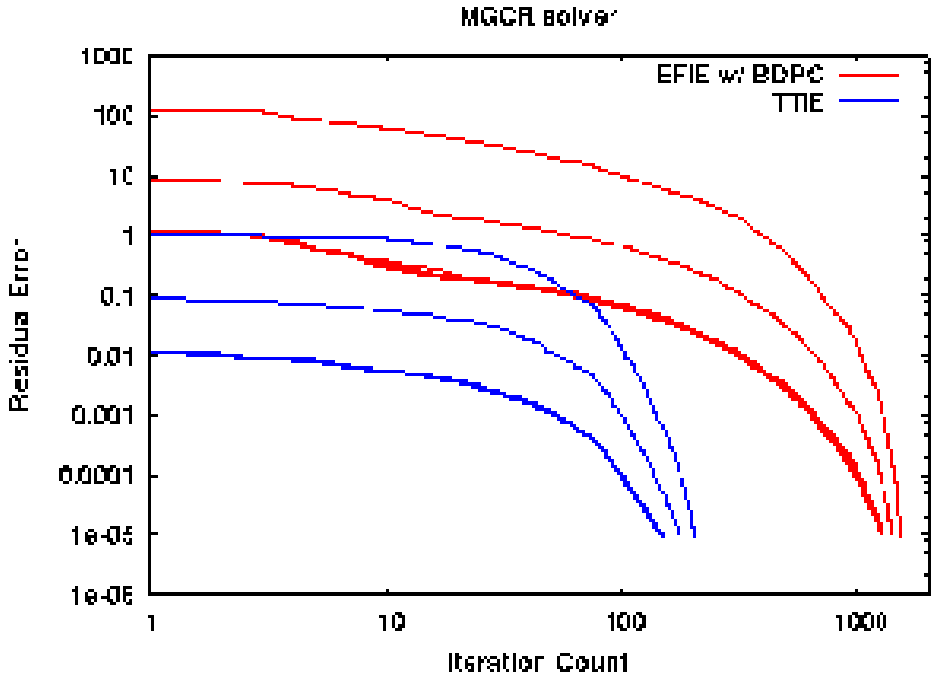

Figure 11: Iterative solver convergence on triangle-circle target using MGCR solver and EFIE (with a block diagonal preconditioner) and the open surface APEFIE.

Circular flat PEC disc target

By virtue of its symmetry and simplicity, the circular flat PEC disc is the canonical open surface PEC target. We investigated the properties of the APEFIE for discs of different sizes. In general, the spectral characteristics of the APEFIE on a disc are similar to those of the APEFIE on the triangle-circle target, in that the eigenvalues are confined to a relatively small region on the negative real half of the complex plane and they tend to cluster about a few points.

We were surprised, however, to find that a few of the eigenvalues converge to the origin when the radius r obeys the condition that kr is a root of J_n, the Bessel function of integer order n. The multiplicity of the eigenvalues at the origin is one for $n = 0$ and two otherwise. For example, the second zero of J_1 is 7.0156. The spectrum of the APEFIE for a disc of radius $R = 7.0156/2\pi$, is shown in Fig. 16. The dot at the origin represents two

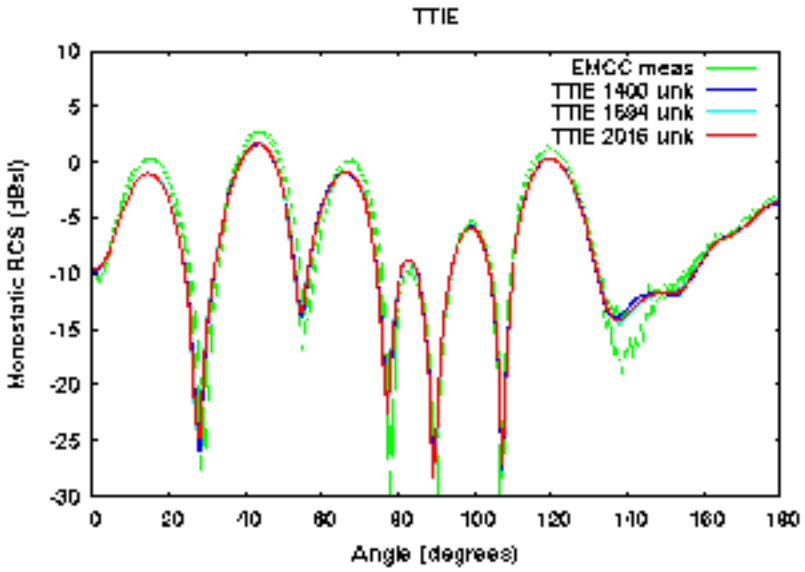

Figure 12: Triangle-circle target RCS: EMCC measurement vs. APEFIE for three different discretizations.

converged eigenvalues.

How do we interpret these zero eigenvalues? Do they correspond to physical resonances on the disc? That possibility is contradicted by the observation that the resonance eigenvalues are not apparent when we use the standard EFIE. Are they spurious resonances? It is well known that solutions to the EFIE for closed targets are susceptible to contamination from spurious resonances, which correspond to solutions to the interior scattering problem. Such solutions are also eigenmodes of the exterior EFIE operator with zero eigenvalues. They do not contribute to the exterior field. However, an open surface such as the disc does not have an interior. The observed resonances seem likely to be spurious resonances of the two open surface APEFIEs we have investigated, although we do not have a simple explanation for why they exist or why they appear under the particularly simple conditions described above.

In the hope of identifying the underlying cause of the resonance eigenvalues and perhaps modifying our APEFIE formulation to avoid them, we attempted to find an analytical series solution to the PEC disc scattering problem. We sought a series solution (analogous to the Mie series solution for scattering from a sphere) in terms of eigenmodes of the APEFIE opera-

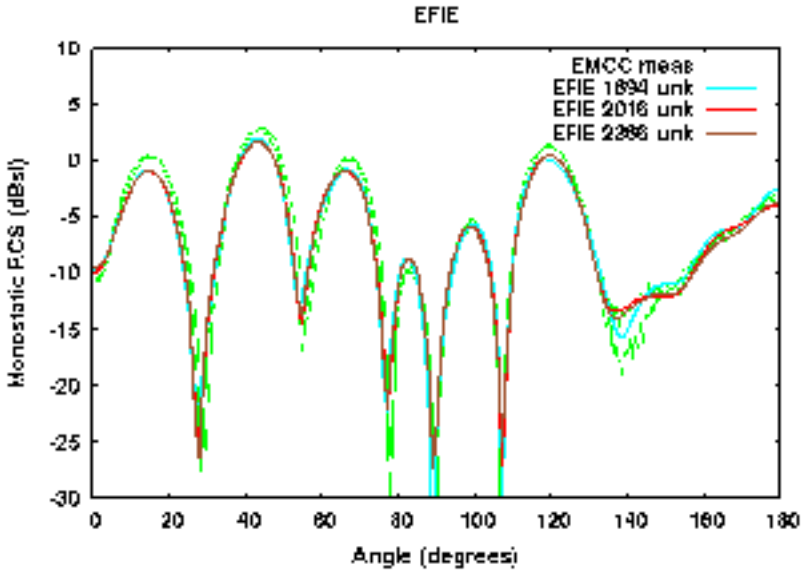

Figure 13: Triangle-circle target RCS: EMCC measurement vs. EFIE for three different discretizations.

tor. We generated a basis set of vector modes on the disc in terms of oblate spheroidal wavefunctions, namely

$$\chi_{lm}(\eta,\varphi;\gamma) \equiv \widehat{\mathbf{n}} \times \nabla\psi_{lm}(\eta,\varphi;\gamma)$$
$$\upsilon_{lm}(\eta,\varphi;\gamma) \equiv \nabla\left(\eta^2\psi_{lm}(\eta,\varphi;\gamma)\right)$$

where $\psi_{lm}(\eta,\varphi;\gamma)$ is the $3d$ scalar Helmholtz mode defined in (37) and $l+m$ is odd. The χ_{lm} vector basis functions can represent surface vector fields with no surface divergence whose azimuthal (radial) component scales like η^{-1} (η) near the edge. The υ_{lm} vector basis functions can represent surface vector fields with no surface curl whose radial (azimuthal) component scales like η (η^3) near the edge. The $3d$ vector Helmholtz equation is not separable in spheroidal coordinates, so it is not obvious what the best choice of vector basis set is.

We derived a set of conditions for the series solution coefficients in terms of some generic $1d$ integrals of products of oblate spheroidal wavefunctions that one can evaluate numerically for any given value of the dimensionless scale size γ.

Late in the program, we realized that it would be possible to analyti-

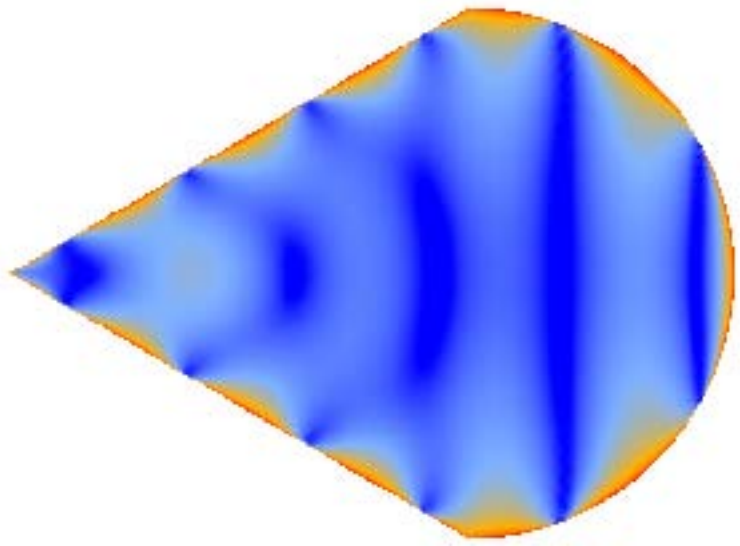

Figure 14: Current distribution on triangle-circle target computed using APEFIE.

cally determine whether or not our APEFIE was a second kind operator by analyzing its behavior in the $k \to 0$ limit where the oblate spheroidal wavefunctions reduce to analytically-expressible associated Legendre functions. The keys to achieving second kind behavior are the terms

$$\frac{1}{\eta}\int_S ds'\,\widehat{\mathbf{n}}\times\nabla G\left(\mathbf{x},\mathbf{x}'\right)\eta'\int_S ds''\,\widehat{\mathbf{n}}'\times\nabla' G\left(\mathbf{x}',\mathbf{x}''\right)\cdot\widehat{\mathbf{n}}''\times\nabla''\psi_{lm}\left(\eta'',\varphi'';\gamma\right) \quad (53)$$

and

$$\eta\,\widehat{\mathbf{n}}\times\int_S ds'\,\widehat{\mathbf{n}}'\times\nabla' G\left(\mathbf{x},\mathbf{x}'\right)\frac{1}{\eta'}\int_S ds''\,\nabla' G\left(\mathbf{x}',\mathbf{x}''\right)\cdot\nabla''\left(\eta''^2\psi_{lm}\left(\eta'',\varphi'';\gamma\right)\right). \quad (54)$$

Using Mathematica, we were able to analytically evaluate expressions (53) and (54) for

$$\psi_{lm}\left(\eta'',\varphi'';\gamma=0\right)\equiv P_l^m\left(\eta\right)e^{im\varphi}$$

with $l+m$ odd. We found that for $m=0$, the spectra of both operators are second kind with an asymptotic eigenvalue collection point at $-\frac{1}{4}$. For

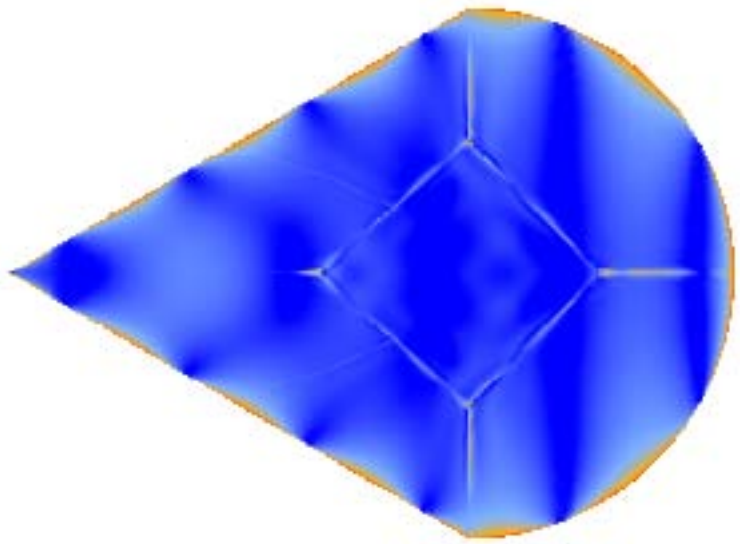

Figure 15: Current distribution on triangle-circle target computed using EFIE.

all other values of m, however, the range of each operator was bigger than the domain, so it was not a closed system and we were not able to construct eigenfunctions with our basis set.

Nonetheless, we did investigate a modification to the APEFIE that showed some promise for eliminating resonance eigenvalues. Not only must the tangential component of the electric field vanish on the surface of a PEC, so also must the normal component of the magnetic field. Therefore, the source distribution must obey the following constraint on the normal component of the magnetic field:

$$\widehat{\mathbf{n}} \cdot \mathbf{H}^{inc} = -\widehat{\mathbf{n}} \cdot \mathbf{H}^{scat} = -\widehat{\mathbf{n}} \cdot \int_S ds' \; \nabla G\left(\mathbf{x}, \mathbf{x}'\right) \times \mathbf{J}\left(\mathbf{x}'\right). \tag{55}$$

At any given source point, the APEFIE applies two constraints on the two components (one for each surface direction) of the source distribution. Eq. (55) places an additional constraint on the two source components. One could solve the over-constrained system of equations described by the APEFIE and (55) (i.e., three constraints, two unknowns) or solve the evenly determined system of equations formed by adding (55) to one or both of the APEFIE component equations (i.e., two constraints, two unknowns). We investigated the latter approach.

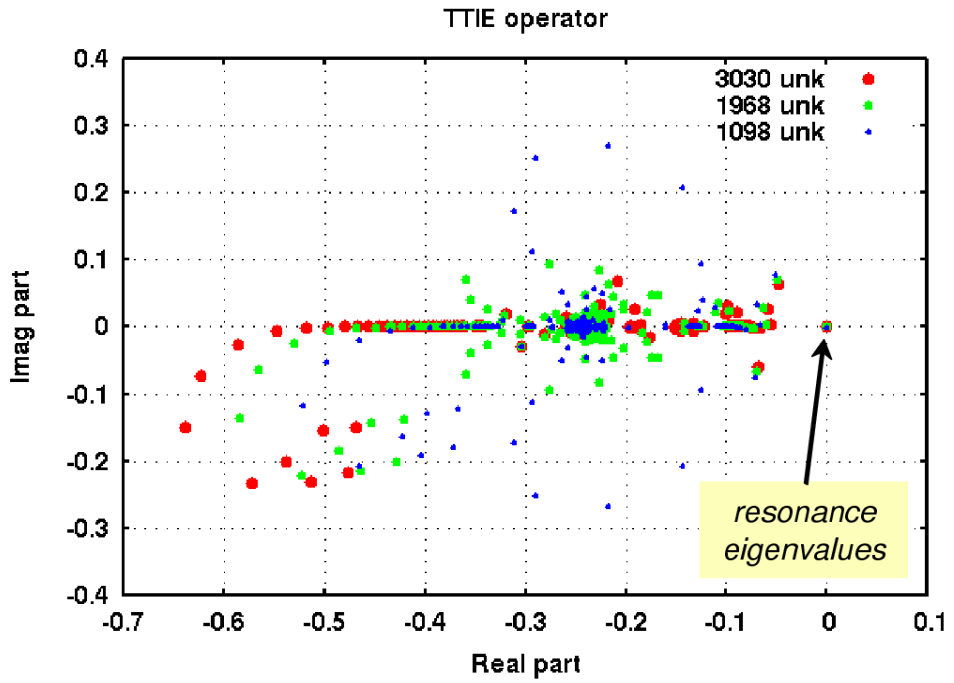

Figure 16: Eigenvalues spectrum for APEFIE on a PEC disc with a "resonant" radius.

The spectrum of the resultant equation is shown in Fig. 17. Adding the normal magnetic field constraint has the salutary effect of shifting the resonance eigenvalues away from the origin. However, it also results in a more widely dispersed spectrum, which is likely to have a deleterious effect on the iterative converge rate. Nonetheless, this version of the APEFIE represents a major improvement over the conventional EFIE in terms of condition number and iterative solver reliability.

8 Discussion

Although we seem not to have found the *ideal* analytic preconditioner for the EFIE on open surface PEC targets, we have found one that is practical to implement numerically and that drastically improves the condition number of the linear system. A few of the practical implications and applications of this achievement are discussed below.

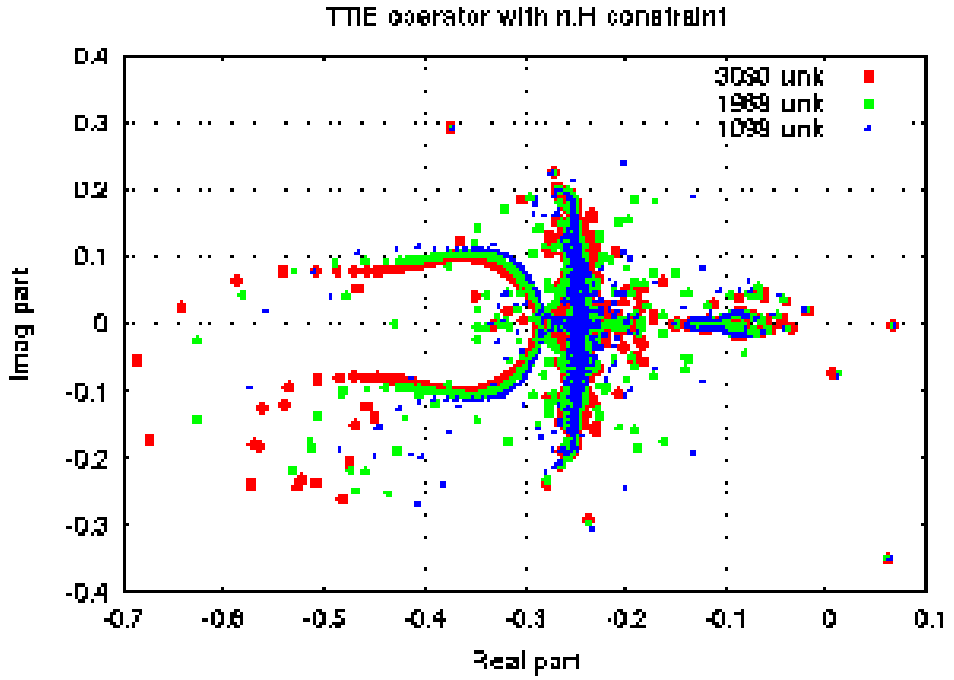

Figure 17: Eigenvalue spectrum of APEFIE + constraint on the normal component of the magnetic field.

8.1 Implications

- *Discretization independence.* Although our implementation is based on a Nyström discretization, it could equally well have been done using a different discretization, such as Galerkin.

- *Time savings.* The purpose of this program is to investigate analytic preconditioners for open surface PEC targets and demonstrate on small test targets how an APEFIE improves iterative solver performance as a consequence of regulating the operator (i.e., improving its condition number). The real domain of practical applicability of an APEFIE is on large targets for which iterative solvers in conjunction with fast methods are a practical necessity and the time spent in the iterative solver phase dominates the overall solution time. Many targets of practical interest fall into this category.

- *Near field accuracy improvements.* Currents computed using the EFIE

usually show the most visible discontinuities at patch boundaries even under conditions where the far field has converged to high accuracy. The underlying reason is that the EFIE operator is hypersingular. The APEFIE, being based on a second kind operator, generally produces noticeably smoother surface currents. Smoother currents should improve the accuracy of derived near field quantities such as port impedances.

- *Dual surface method applied to the EFIE.* The dual surface integral equation method [11] is a straightforward, general technique for eliminating spurious resonances in closed surface scattering problems. It does so by adding a term derived from a particular compact operator to the original equation. There was no particular benefit in using this method with the EFIE because the resulting equation would still be ill conditioned. However, it does make sense with the APEFIE because the APEFIE is well conditioned and it stays that way even after the dual surface component is added on. Thus a dual surface APEFIE is worth considering as an alternative to the CFIE on closed surface PEC targets.

8.2 Applications

- *EM scattering calculations.* The APEFIE is useful for solving scattering problems involving both open and closed PEC targets, but is especially valuable on large open surface targets due to the lack of practical alternatives.

- *Quasi-static EM analysis.* Since the APEFIE is well conditioned from high frequencies down to DC, it could be used to analyze quasi-static EM problems (such as motors) for which the EFIE is not a good analysis tool because of ill conditioning.

- *Scalar/acoustic scattering.* It is obvious from the analysis of the flat circular disc in Section 7.1.2 how to construct an ideal analytic preconditioner for scalar scattering from an open surface target under Dirichlet or Neumann boundary conditions. One could solve large, open surface acoustic scattering problems involving acoustically hard or soft surfaces this way.

8.3 Conclusions

A long-standing problem with the integral equation approach to modeling very thin metal structures in the frequency domain is that the choice of integral equation is limited to the inherently ill conditioned EFIE. For large scattering problems, one would like to be able to speed up the calculation by using iterative solvers in conjunction with fast solver methods (such as the FMM), but the requirement to use the EFIE makes this impractical in many cases. The general purpose matrix preconditioners that have been applied to address this problem operate with varying degrees of reliability and computational efficiency.

The ideal solution would be an inherently well conditioned, second kind integral equation suitable for use on open surface PEC targets. The analytic preconditioner developed and investigated under this program comes very close to attaining this goal. Depending on your point of view, we have either found a well tuned preconditioning operator for the EFIE or a new, well conditioned integral equation to augment the EFIE.

We implemented an analytically preconditioned EFIE (APEFIE) that stabilized and dramatically improved iterative solver performance as compared to conventional numerical preconditioning methods when applied to simple test targets. For example, the number of iterations required to achieve solution convergence on the EMCC triangle-circle target fell from $\sim$50000 for the standard EFIE with a conventional block diagonal preconditioner to $\sim$30 with the APEFIE. Similar results were obtained on other small open surface test targets. The most significant benefits in terms of computational savings will be observed when an fast method version of the APEFIE is applied to large open surface targets.

The underlying reason for the iterative solver performance improvement can be found in the eigenvalue spectrum of the integral operator. The APEFIE has a second kind spectrum, with eigenvalues corresponding to high spatial frequency eigenmodes tending to cluster about a few collection points well separated from the origin. At the origination of this program we suspected that it would be a nontrivial task to actually achieve such a spectrum in a numerical implementation and we proposed to use a $2d$ version of the Poincaré-Bertrand identity (PBI) to make this task easier. Early on we numerically validated the $2d$ PBI, but as the program progressed, we found an alternative, less cumbersome means to achieve the same objective so we abandoned the $2d$ PBI approach.

Our investigation showed that under some circumstances the APEFIE spectrum can include a small number of zero eigenvalues, which are reminis-

cent of the spurious resonances known to plague the EFIE for closed surface PEC targets. To understand this problem we attempted to obtain an analytical solution for the spectrum of the APEFIE on the canonical open surface target, a circular disc. We made some progress in this direction (as reported here), but in the end, did not fully realize this goal or arrive at a satisfactory understanding of the reason for the zeros in the spectrum. One hopes that a more complete analysis will bring forth an even better APEFIE for which these zero eigenvalues do not exist.

References

[1] H. Contopanagos, B. Dembart, M. Epton, J. J. Ottusch, V. Rokhlin, J. Visher, and S. Wandzura. Well-conditioned boundary integral equations for three-dimensional electromagnetic scattering. *IEEE Transactions on Antennas and Propagation*, 50(12):1824–1830, December 2002.

[2] Tongde Zhong and Lüping Chen. The Poincaré-Bertrand formula for the Bochner-Martinelli integral. *Integr. equ. oper. theory*, 54:585–595, 2006.

[3] Shidong Jiang and Fengbo Hang. Generalized Poincaré-Bertrand formula on a regular surface in three dimensions. Technical Report CAMS Report 0506-13, 2006.

[4] N. I. Muskhelishvili. *Singular Integral Equations: boundary problems of function theory and their applications to mathematical physics (English translation)*. Wolters-Noordhoff, Gröningen, 1953.

[5] Robert J. Adams and Gary S. Brown. Stabilisation procedure for electric field integral equations. *Electronics Letters*, 35(23):2015–2016, November 1999.

[6] Peter Kolm and Vladimir Rokhlin. Quadruple and octuple layer potentials in two dimensions I: Analytical apparatus. Technical Report YALEU/DCS/RR-1176, Yale University, Department of Computer Science, March 1999.

[7] Shidong Jiang and Vladimir Rokhlin. Second kind integral equations for scattering by open surfaces I: Analytical apparatus. Technical Report YALEU/DCS/RR-1233, Yale University, Department of Computer Science, August 2002.

[8] Shidong Jiang and Vladimir Rokhlin. Second kind integral equations for scattering by open surfaces II. Technical Report YALEU/DCS/RR-1244, Yale University, Department of Computer Science, January 2003.

[9] Jason Cantarella, Dennis DeTurck, and Hermann Gluck. Vector calculus and the topology of domains in 3-space. *Amer. Math. Monthly*, 109(5):409–442, 2002.

[10] George C. Hsiao and Ralph E. Kleinman. Mathematical foundations for error estimation in numerical solutions of integral equations in electromagnetics. *IEEE Transactions on Antennas and Propagation*, 45(3):316–328, March 1997.

[11] M. B. Woodworth and A. D. Yaghjian. Multiwavelength three-dimensional scattering with dual-surface integral equations. *J. Opt. Soc. Am. A*, 11(4):1399–1413, 1994.

[12] Carson Flammer. The vector wave function solution of the diffraction of electromagnetic waves by circular disks and apertures, part i: Oblate spheroidal vectorsw ave functions; part ii: The diffraction problem. *J. Appl. Phys.*, 24, 1953.

[13] Lawrence S. Canino, John J. Ottusch, Mark A. Stalzer, John L. Visher, and Stephen M. Wandzura. Numerical solution of the Helmholtz equation in $2d$ and $3d$ using a high-order Nyström discretization. *Journal of Computational Physics*, 146:627–663, 1998.

[14] Milton Abramowitz and Irene A. Stegun. *Handbook of Mathematical Functions*. Applied Mathematics Series. National Bureau of Standards, Cambridge, 1972.

[15] I. S. Gradshteyn and I. M. Ryzhik. *Table of Integrals, Series, and Products*. Academic Press, Inc., San Diego, corrected and enlarged edition, 1980.

[16] Phillip M. Morse and Hermann Feshbach. *Methods of Theoretical Physics*. McGraw-Hill, New York, 1953.

List of Acronyms

EFIE	Electric Field Integral Equation
MFIE	Magnetic Field Integral Equation
APEFIE	Analytically Preconditioned Electric Field Integral Equation
TTIE	T-squared Integral Equation (synonymous to APEFIE)
FMM	Fast Multipole Method
EMCC	Electromagnetic Code Consortium
PBI	Pointcaré-Bertrand Identity
RCS	Radar Cross-Section
PEC	Perfect Electrical Conductor